LINE BLANKETING EFFECTS ON MIDDLE-TYPE MAIN-SEQUENCE AND SUB-DWARF STARS

Thesis by

William Geary Melbourne

In Partial Fulfillment of the Requirements

For the Degree of

Doctor of Philosophy

California Institute of Technology

Pasadena, California

1959

ACKNOWLEDGEMENTS

It is with sincere gratitude that I thank Dr. Arthur D. Code who suggested the problem of line blanketing -- its effects on measured energy distributions and colors -- and its role in sub-dwarf stars. Dr. Code acted as thesis advisor during his tenure at the Institute and has continued during the past year while director of the Washburn Observatory to supply guidance and advice of inestimable value.

I wish also to express gratitude to Drs. Greenstein and Oke for their discussions with me concerning this work.

Finally, to Dr. George Abell of U.C.L.A., I owe special thanks for obtaining at rather short notice the colors of HD140283.

ABSTRACT

The subject of line blanketing and its effect on the continuous radiation and measured colors of stars is reviewed. Observed energy distributions which have been corrected for blanketing are compared with theoretical flux distributions derived from model atmospheres. Reasonable agreement is found and the comparisons serve to establish a set of effective temperatures for the stars under study.

The UBV colors of the program stars are computed from the observed energy distributions and the results are compared with the observed colors. The theoretical colors are also obtained. The effects of line blanketing with and without the hydrogen lines on the UBV colors are quantitatively assessed. A three dimensional (U-B) — (B-V) — effective temperature relationship is discussed. The above analysis leads to line-free UBV and color-magnitude main-sequence relationships.

TABLE OF CONTENTS

I. INTRODUCTION

1. Discussion

In problems concerning the spectral distribution of the stellar radiation, a valuable theoretical approach is the use of a model stellar atmosphere constructed with the available knowledge of the physical processes in stellar atmospheres. The variable parameters of the model are adjusted to coincide with the estimated values in the real atmosphere. To keep the problem tractable, several simplifying assumptions of varying degrees of departure from reality are introduced into the model structure. The temperature distribution through the atmosphere derived from the solution of the grey atmosphere problem in radiative equilibrium is commonly used with the hydrostatic equation and the subsidiary ionization and opacity relations to describe the run of the physical properties of the gas with depth in the atmosphere. With this information the observable features of the radiation field in the atmosphere are computed and compared with observation. The ability of the model atmospheres method to predict many of the spectral features in fair agreement with observation would seem to indicate both its usefulness as an analytical tool and the accuracy of our knowledge of the basic physical theory of interaction between matter and radiation in the stellar atmospheres. On the other hand, the disparity in certain instances between theory and precise observation, particularly in some spectral features which are sensitive to the model structure sharply points up the shortcomings of some of the approximations employed.

In the construction of such models it is implicitly assumed that a separation between the continuous and discrete opacities may be effected without seriously distorting the model. The temperature distribution through an atmosphere generally in radiative equilibrium is derived by considering a grey or mean opacity; in more sophisticated treatments this distribution may be refined by including the departure from greyness of the continuous opacity alone and requiring flux constancy. Because of the extreme complexity of the combined opacities the discrete opacity is nearly always neglected at this phase of the problem. Moreover, the discrete opacity is again neglected in computing the continuous radiation field in the atmosphere and it is only after these features have been established that the discrete opacity is applied in localized spectral regions in order to compute, for example, the profiles or strengths of particular absorption lines. It is apparent that this

separation gives rise to two types of disparity between the model and the real atmosphere. The presence of absorption lines in the real atmosphere modifies the temperature distribution leading to an observable monochromatic flux whose continuum may differ from the continuous flux of the model and which possesses the absorption lines neglected in the model.

There exists an analogous problem in the observational approach to the spectral distribution of stellar radiation. It is not feasible both from the standpoint of telescope economics as well as instrumentation complexity to obtain the distribution of monochromatic flux from a star with a sufficient purity to accurately measure the profiles of absorption line and at the same time cover the whole observable spectral region. Consequently, the observational approach in the extremes is either to investigate a limited spectral region with a fine band pass such as with a spectrograph or to use wide band passes to cover broad areas of the spectral distribution with little attempt to discern the fine structure within each band. The UBV photometric system may be considered as an example of the latter.

To a large extent, it is because of this analogous feature in observational technique that we are particularly hindered in continuous stellar radiation measurements by the presence of absorption lines. A more serious problem than that due to the limited resolving power of our instrumentation is the crowding of absorption lines in the ultraviolet regions of late-type stars causing a real suppression of the continuum. Certainly in very cool stars, the overwhelming presence of absorption lines must vitiate this formal separation of continuous and discrete opacities and indeed render the concept of a continuous opacity rather meaningless. But for stars such as the sun and earlier this separation does not seem to have caused serious discrepancies in regions relatively free from absorption lines nor in studies of absorption line profiles; although, it may be argued that the neglect of the blanketing effect upon the temperature distribution may create problems in the study of the profiles of lines since the change in the temperature distribution is greatest at small optical depths.

ii. Theoretical Blanketing Studies

Historically, the effect of the presence of absorption lines on the temperature distribution was known as the problem of line blanketing.

Nowadays however, this term is often applied categorically to all problems arising from the separation of continuous and discrete opacities in model atmospheres analysis. The various theoretical studies of the blanketing effect on the temperature distribution through the atmosphere have used different approaches which are necessarily idealized. Milne (1921) considered the effect of absorption line formation in a thin scattering layer situated above a grey photosphere in radiative equilibrium which acted as a blanket to increase the temperature in the atmosphere. Chandrasekhar (1936) assumed a formation of absorption lines of equal intensity by absorption and scattering processes occurring in constant strength throughout the atmosphere. The absorption lines were uniformly distributed across the spectrum and the Eddington approximation was used to solve the problem. Münch (1946) solved the same problem using the refined methods of Chandrasekhar for solution of the transfer equation. For the formation of lines by pure absorption he also considered the case where the frequency distribution of line occurrence was arbitrary. In these studies the emphasis has been on the sun where the theoretical temperature distributions may be compared with the results obtained from limb darkening measures. More recently, others have studied the problem using a variety of methods; but in all these studies which contain conditions resembling those in a real atmosphere there is a consistent similarity in the pattern of the blanketing modified temperature distribution curve. If one plots the fourth power of the temperature against mean optical depth one obtains for the grey atmosphere a curve which rises from the boundary value, T_o^4, with diminishing curvature and which eventually approaches a straight line with a slope of $\sqrt{3}T_o^4$. For a grey atmosphere model of the sun the blanketing modified distribution begins at the boundary several hundred degrees below the standard model, progresses very steeply upward intersecting the standard curve around $\tau = 0.1$, then turns more or less parallel to the standard curve by $\tau = 0.2$ and proceeds in this manner for greater optical depths at a temperature higher by 100 - 200° k. This observation leads to an important conclusion which forms a working hypothesis of this thesis. Although the additional curvature in the temperature curve may have a considerable effect on the cores of strong lines and on limb darkening measures the spectral distribution of the continuous flux should be relatively insensitive to this departure from the

standard atmosphere curve for stars with moderate blanketing (viz. 10%) or less. However, the continuous monochromatic flux in the real atmosphere should correspond to a model with a higher effective temperature than the true effective temperature of the star because of the flux removed by the lines. This conclusion follows from the fact that the great majority of the flux contributing to the continuum at the surface originates from optical depths greater than 0.2.

There is the further complication that ΔF, the amount of flux removed by the lines in a real atmosphere is surely not independent of optical depth as assumed in these theoretical studies. Labs (1951) and Pecker (1950) have attempted to evaluate $\Delta F(\tau)$; however, the problem is very difficult. Because there is no accurate knowledge of the variation of this quantity with optical depth, in studying solar models the surface value of this quantity is generally taken to hold throughout. It does not seem, however, that the general conclusions concerning the blanketing perturbed temperature curve should be altered by this effect. In his original blanketing study Chandrasekhar (1936) also considered the problem of an atmosphere in which absorption lines may occur down to an optical depth τ_o, after which there is only continuous opacity. The resulting temperature distribution of this two-layered atmosphere possesses the same characteristics of other blanketing temperature curves.

iii. The Present Study

In this study a family of monochromatic continuous flux curves has been computed from a set of model atmospheres. The grey atmosphere temperature distribution in radiative equilibrium along with the available knowledge of the source of continuous opacity and the hydrostatic equilibrium equation were used to construct these models. The values of the surface gravity used correspond to middle-type main-sequence stars and the hydrogen to metals ratio A, was taken as $\log A = 3.8$. No attempt was made to refine these models for departures from greyness, line blanketing, constancy of flux, etc. Concerning the latter, flux constancy holds to around 5% for these models; furthermore, it is not clear that this is a valid requirement since these models become convectively unstable at varying depths. However, it is well known that the flux distribution is rather insensitive to all of these effects

as well as to moderate variations in the surface gravity; moreover, departures of the continuous opacity from greyness are not large for the later spectral types. In regard to flux constancy and convection, Swihart (1956ab) has constructed two models corresponding to a solar and an F5 atmosphere with the flux constancy condition fulfilled. He also constructed a solar model with convective instability commencing around $\tau = 1.0$ with 40% of the energy being transported by convection at $\tau = 3.0$. The monochromatic fluxes derived from these models may be compared with the fluxes obtained in this study. It can be shown that the differences between them is less than the uncertainties in the observations which will be discussed later. Swihart (1956c) also constructed a solar and an F5 atmosphere with $\log A = 5.0$. A comparison between monochromatic fluxes of these models and his $\log A = 3.8$ models reveals the expected result of almost negligible differences. It would follow, then, that the models in this study should also be applicable to F-type metals-deficient sub-dwarf stars.

A varying abundance of metals among the stars produces:

1. a differing continuous opacity in the atmosphere by a variation of the electron pressure,
2. a different amount of line absorption in the emitted monochromatic flux,
3. possibly a difference in the radius and luminosity and therefore the effective temperature through an alteration of the internal structure.

To the extent of our knowledge of the opacity and energy sources in the stellar interiors we may predict the manner in which the effective temperature and luminosity depend on chemical composition. Schwarzschild (1958) has discussed the changes in the configurations of cool stars with a metals deficiency such that the interior opacity arises from free-free hydrogen and helium absorption processes and electron scattering rather than from bound-free metallic absorption. The departure of the sub-dwarf from the main-sequence line in the Hertzsprung-Russell plane is in the right direction but is shown to be sensitive to the helium abundance. He also considers in a general way the dependence of the configuration on the depth of a convection envelope which strongly affects the radius of a star. However, at the present time it is not certain the bound-free process predominates in the cores

of stars of normal abundances (Naur 1954); if the free-free process is the rule the effect of a metals deficiency on stellar configurations maybe mitigated.

The spectral distribution of the emergent flux is altered through these internal structure changes. Besides this, the distribution is altered because of the atmospheric effects listed above. Since electron pressure changes are known to produce little effect on the distribution of the emerging flux (Cf. De Jager and Neven 1957) it remains to consider the effect of differing line absorption.

A primary motivation for this study is to assess the effect of line absorption on the measured colors of stars of different spectral type and chemical composition. The colors of a star are determined by the spectral distribution of the continuous flux and by the amount of line absorption occurring in the band passes defining the color system. The spectral distribution of the continuous flux is in turn affected by line absorption through the blanketing effect and as indicated above, depends almost solely on the extent to which the temperature distribution curve is elevated above the standard curve. Although the flux removed by the lines is variable with optical depth, the amount of line absorption at the surface of the atmosphere largely determines the elevation of the temperature curve over the standard curve because nearly all the energy removed by the lines is redistributed through the continuous spectrum and because the flux in the lines emitted at the surface originates from atmospheric layers which contribute little to the continuous flux. Therefore, to good approximation the true effective temperature of a star T_e, and T'_e, the temperature describing the continuous monochromatic flux are connected by the relation

$$\sigma T_e^4 = \sigma T_e'^4 - \Delta F(0). \tag{1}$$

With the proper model temperature selected one may then compare theory and observation in the blue and ultraviolet regions where line absorption becomes more pronounced. In these regions the observed monochromatic flux is depressed by absorption lines due to the finite band-width of the receiver used in these measurements. To compensate for this one may use high dispersion spectra to measure the amount of blanketing within each band pass of the spectral

distribution covered by the receiver. If line absorption is not so severe that it suppresses the continuum these measures yield quantities with which the receiver deflections may be corrected to obtain the flux in the absence of absorption lines. The receiver used in these flux measurements is a photoelectric scanning spectrograph whose band pass is nominally about 15A. The details of this instrument are given in the following chapter. The goodness of fit of the continuous spectral features in the blue and ultraviolet regions between the theoretical flux and the blanketing compensated observed flux is a measure of the precision of the observations and of the accuracy of our knowledge of the processes giving rise to the monochromatic continuous flux in these spectral regions.

At this point one may also study the effects of blanketing on stellar colors. From an observational standpoint, a reference photometric system may be considered as one which is defined by a list of standard stars whose colors are measured in this system. Other photometric systems may be related to this reference system by including some of these standards in their observing programs. An alternate approach defines this photometric system physically by specifying the response functions of the various adopted filter systems. One may write the response, R(A), of a filter system A, as

$$(2) \qquad R(A) = \int F_\nu \cdot S_\nu \ (A) \cdot d\nu \quad ,$$

where F_ν is the monochromatic flux and S_ν (A) is the response function. By employing two or more filter systems the color or colors of a star are determined with respect to the set of filter systems used. In this manner the published values of the response functions of the Johnson-Morgan UBV photometric system (1953) may be used to determine the U-B, B-V colors of a star from the observed monochromatic flux. These computed colors should agree with the observed colors. At this point, by performing the above integrations using the observed and the blanketing compensated monochromatic fluxes one may also establish the effect of line blanketing on the observed colors.

By studying stars of diverse spectral type and chemical composition one may use the above methods to ascertain the dependence of the blanketing color effect on these two factors thus affording another dimension to our

stellar classification scheme. In this study the following stars have been used:

Name	HD	Type	M_V	(1950)	
α Lyr	172167	A0 V	0.14	18-35-15	38 44.2
γ Ari	11636	A5 V	2.72	1-51-52	20 33.9
σ Boo	128167	F2 V	4.48	14-32-30	29 57.7
π^3 Ori	30652	F6 V	3.31	4-47-07	6 52.5
110 Herc.	173667	F6 V	4.26	18-43-31	20 29.8
β Com.	114710	G0 V	4.32	13-09-32	28 07.9
51 Peg.	217014	G4 V	5.59	22-55-00	20 30.0
	140283	F type sub-dwarf	7.26	15-40-22	-10 46.3
	19445	F type sub-dwarf	8.0	3-05-29	26 09.1

The star HD19445 probably represents a typical F-type sub-dwarf while HD 140283 is more extreme being very deficient in metals abundance.

In the following chapters the details of the observational techniques and model atmosphere constructions are discussed. A comparison of theory and obeervation and the blanketing effect on the colors follows.

II. OBSERVATIONAL TECHNIQUES AND MEASUREMENTS

The observations in this study may be categorized into two kinds: the spectral distribution and the line absorption measurements. Since there is little information published on the particular instrumentation and technique used to obtain monochromatic fluxes these topics are discussed below in some detail.

I. Spectral Distribution of Stellar Fluxes.

1. Equipment

The instrument used in this study is known as a photoelectric scanning spectrograph. This particular receiver designed by Code measures the spectral distribution of stellar energy with an optimum purity of about 15A. It accepts an f/16 light bundle which means it is adapted to operate at the Cassegrainian focus of the 60-inch, 100-inch and 200-inch telescopes.

Since this instrument records the incident flux at varying wavelengths as a function of time it is mandatory that the time series fluctuations in the recorded flux be minimized. Consequently, the total light pencil forming the image enters the entrance slit or diaphram; for, if any part of the pencil is obscured the fluctuations due to seeing cause the amount of obscuration to vary. Even under excellent seeing conditions the slight obscurations cause recorded fluctuations well beyond the tolerable limit. The entrance aperture therefore serves only to reduce the effect of background light and to define the area over which a light beam will fully strike the Fabry lens in the photomultiplier assembly.

The f/16 light bundle proceeds through the entrance aperture to the upper part of a 32-inch focal length, 6-inch spherical mirror where it is collimated and returned to the grating. From the grating the parallel bundle of the proper wavelength interval returns to the lower half of the 6-inch mirror where it is focused via a prism at the exit slit. After passing through the exit slit the bundle proceeds through any necessary filters and is customarily brought to a photomultiplier assembly. The signal from the photomultiplier is amplified and generally recorded on tracing paper. The wavelength scale on the tracing paper may be calibrated by a wavelength meter on the scanner or by obvious spectral features in the tracing. The details of the photoelectric equipment are widely known; therefore little discussion will follow about this phase of the observations.

Although a paraboloidal mirror is required to strictly collimate the light bundle, at this focal ratio of f/16 the departures of the collimated beam from parallelism using a spherical mirror are insignificant. Using one spherical mirror avoids the requirement of two mirrors for collimation and focusing. The incoming bundle, although off-axis, utilizes only a 2-inch portion of the 6-inch mirror; it may be shown for these circumstances that a parallel beam produces a spurious image whose diameter is a few percent of the exit slit width thus negligibly affecting the band width.

For stars, the band pass of the scanner is regulated by the exit slit and the size of the stellar image at the entrance slit. Therefore, for a given focal ratio the seeing and the telescope aperture determine to some extent the purity of the measured spectral distribution. At the 100-inch telescope with average seeing the minimum band width which occurs with an infinitesimal exit slit width is about 5A. The spectral distribution of the energy within this band width possesses about the same shape as the distribution of starlight in the image plane of the telescope; as the exit slit is widened the spectral distribution, of course, becomes broadened. There is a minimum width of the exit slit while scanning in order to avoid distortions in the tracings. This width is determined by the rate of scanning and the time constant of the amplifier. The time required for a wavelength mark to cross the band pass should be around five times the time constant of the amplifier. A convenient scanning rate often used is 200A/min; this allows five seconds for a wavelength mark to cross a 15A band pass which implies a time constant of about one second — a typical value for the D.C. amplifiers used in photometry. The scanning is accomplished by rotating the grating with a synchronous motor through a set of gears some of which may be exchanged to change the scanning rate. The grating has 15,000 lines/inch and is blazed at 4000A in the second order. This gives a dispersion at the exit slit of 10A/mm which with an exit slit width of 1mm gives a band width of about 15A. In working in the red and infrared regions it is better to use the first order spectrum of the grating in order to receive the benefit of the 8000A blaze. In this case the minimum band width increases accordingly; however, in these regions a band width of 30A is quite tolerable since the quantity $\Delta\lambda/\lambda$ is held to the same order of magnitude.

The spectral distribution from 3000A to 10,000A may be obtained using a photomultiplier with an antimony-cesium surface (S4) such as a 1P21 tube

in the 3000A to 6000A range and a cesium oxide on silver surface (S1) which is sensitive to 10,000A. The new multialkali surfaces have a range from 3000A to 8000A and have the advantage of being more sensitive than the S1 surfaces.

In most of the spectral regions covered a filter must be employed to cut out the overlapping orders of the grating. In the second order a yellow filter such as a GG5 is used from 4600A on to cut out the third order radiation. Similarly, in the red regions an amber filter such as a Schott OG1 is used to cut out the second order radiation. Since in general two different photomultipliers sensitive to different spectral regions are employed it is necessary that a proper selection of the filters be made in order to have overlapping spectral regions covered by both tubes. The amber filter used in the red regions has a cut-off at 5400A thus allowing the region between 5500A and 6000A to be covered by both the S4 and the S1 surfaces. The overlap is necessary because the energy measurements across the whole spectral range are made relative to the energy at one wavelength — generally 5560A. The yellow filter cutting off at 4600A suffices when one is using the multialkali surface in conjunction with a 1P21 to cover the 3000A - 8000A range.

ii. Observational Methods

The observational techniques used with the scanner are similar to wide band photoelectric photometry techniques. In both approaches one measures in a particular band pass the response of the system to the incident radiation; the aim being to obtain this response corrected to outside the terrestrial atmosphere relative to the response from a standard star. With the scanner one is primarily interested in the spectral distribution; consequently, it is only necessary to obtain the distribution of energy relative to the energy within a particular band pass. The band pass customarily chosen is centered at 5560A for the reason indicated above. The fact that an absolute determination of the stellar energy curve is unnecessary in determining the shape of the energy distribution relaxes some of the observational problems.

The quantities involved in the scanning observations are now considered in a somewhat quantitative manner. The integral effective intensity I, is defined by

$$(3) \qquad I(\lambda_o) = \int F_\lambda \cdot s_\lambda(\lambda_o) \cdot P_\lambda(z)\, d\lambda \,, \qquad ,$$

where F_λ is the monochromatic flux at the top of the terrestrial atmosphere; $s_\lambda(\lambda o)$ is the normalized sensitivity function of the band pass centered at λo and $p_\lambda(z)$ is the atmospheric extinction and is a function of the zenith distance z. The integral effective intensity is, then, the response of the instrument and is proportional to the deflection of the recorder. The integral effective intensity reduced to outside the atmosphere is

$$(4) \qquad I_o(\lambda o) = \int F_\lambda s_\lambda(\lambda o) d\lambda \quad .$$

Since the atmospheric extinction is essentially constant within the band pass at a particular wavelength equation 3 may be written as

$$(5) \qquad I(\lambda o) = P_{\lambda o}(z) \int F_\lambda s_\lambda(\lambda o) d\lambda \quad .$$

Moreover, except for wavelengths lying in an absorption line F_λ is also very constant within a band pass; in any case equation 5 may be written as

$$(6) \qquad \begin{aligned} I(\lambda o) &= P_{\lambda o}(z) \overline{F_{\lambda o}} \int s_\lambda(\lambda o) d\lambda \\ &= P_{\lambda o}(z) \cdot \overline{F_{\lambda o}} \cdot S(\lambda o) \quad . \end{aligned}$$

If in the standard star the monochromatic flux relative to a reference wavelength $\overline{F}_{\lambda o} / \overline{F}_{\lambda r}$, is known, the relation

$$(7) \qquad I(\lambda o) / I(\lambda r) = F_{\lambda o} \cdot p_{\lambda o}(z) S(\lambda o) / F_{\lambda r} \cdot p_{\lambda r}(z) S(\lambda r) \quad ,$$

affords a way of obtaining the relative flux of the star by measurements of the relative integral effective intensity reduced to outside the atmosphere of both the star under study and the standard star. Unless the measurements of the two stars are made with the same zenith distances, a knowledge of the extinction coefficient is required. With this correction applied to both sets of measurements, the relation between the two sets of relative fluxes may be written as

$$(8) \qquad \left[\frac{F_{\lambda o}}{F_{\lambda r}}\right]_{star} = \left[\frac{I_o(\lambda o)}{I_o(\lambda r)}\right]_{star} \cdot \left[\frac{F_{\lambda o}}{F_{\lambda r}}\right]_{stnd.} \Big/ \left[\frac{I_o(\lambda o)}{I_o(\lambda r)}\right]_{stnd.} \quad .$$

The atmospheric extinction varying with wavelength in the same manner as Rayleigh scattering has the form

$$(9) \qquad p_\lambda(z) = \exp\left\{-\left[A + B/\lambda^4\right] \sec z\right\},$$

where A is a grey term due to non-selective scattering of light by dust particles and therefore depends on the haziness of the atmosphere; B is the Rayleigh scattering coefficient and depends slightly on the atmospheric pressure. The actual extinction expression except for the grey term differs negligibly from the above law from night to night for $\lambda > 4000$A; moreover, as was indicated above the deduced relative fluxes with respect to the standard relative fluxes depend in a second order manner on the values used for the extinction. Since it is the relative extinction with which one is concerned, which for the Rayleigh expression is

$$(10) \qquad p_\lambda / p_{\lambda_r} = \exp\left\{B\left[1/\lambda_r^4 - 1/\lambda^4\right] \sec z\right\},$$

it is only in the ultraviolet regions where the deviations from the above expression due to ozone absorption may be appreciable. It is the error in the adopted relative extinction value multiplied by the difference in secant z values between the two stars that affects the value of the deduced relative fluxes. Accordingly, a standard relative extinction curve has been compiled by Code (unpublished) from many nights of extinction measures over a long period of time. This curve follows the Rayleigh expression very closely for $\lambda > 4000$ and with the exception of spectral regions where atmospheric absorption bands occur, should be at worst within a few percent of the actual curve on any given night. Table I lists points on this curve for sec z = 1 in magnitude units defined by $K_\lambda = -2.5 \log (p_\lambda / p_{5560})$.

The relative extinction coefficient may be determined on a night-to-night basis by the usual photometric procedure of measuring the response from a star at two or more zenith distances. This procedure is somewhat time-consuming because of the number of wavelengths at which this quantity is measured at one time. By restricting observations so that the differences in secant z between the two stars is small (a few tenths, say) one should be able to use the standard curve and expect errors in the flux of no more

than a percent or so in the extreme cases. Both procedures were employed in this study; it was found, however, that unless one was observing a star of large zenith distances the differences between the measured and the standard extinction curves and the uncertainty in the measurements indicated that it was uneconomical to make extensive measurements.

Table I

EXTINCTION COEFFICIENTS

$\lambda(\mu)$	.340	.365	.386	.404	.419	.459	.506	.556
k_λ	.770	.480	.310	.230	.170	.088	.032	.000
$\lambda(\mu)$	.581	.605	.667	.746	.800	.875	.909	1.000
k_λ	-.010	-.020	-.050	-.075	-.085	-.095	-.100	-.110

Up to this point the discussion has been concerned with what is called relative spectrophotometry, that is, the measurement of the monochromatic flux distribution of one star relative to another. In order to obtain the shape of the spectral energy distribution, or in other words, to do absolute spectrophotometry one must know the energy distribution of the standard star. An absolute determination of the shape of the spectral distribution of a standard star to within 1% accuracy, for example, is an exacting and difficult problem which up to the present time has yielded results leaving in certain regions something to be desired. In this calibration of the standard star (or stars) one compares the stellar monochromatic flux with that from a laboratory source which is generally brought through the same optics as the star. The laboratory source must in turn be calibrated. A moderate amount of effort has gone into these two parts of the problem; yet, there remains a third part which contributes as great an obstacle — the atmospheric extinction. It is mandatory that we know the flux outside the atmosphere in order to relate it to the physical theory of stellar atmospheres. In the ultraviolet, time-varying values of the color term as well as the grey term due to varying atmospheric conditions present considerable challenge to the goal of 1% accuracy. A rather comprehensive survey of the problem of absolute calibration and of the efforts which have been made is given by Code (1959). Most of the work has been on α Lyrae although 10 Lacertae and ϵ Orionis because of their blueness and smooth distributions have also

been studied in the ultraviolet.

The quantity $S(\lambda_o)$, is a function of time while scanning and though the the integral effective intensity may be evaluated at any wavelength, in order to satisfactorily define the spectral distribution of a star it is sufficient to reduce the observations at a number of wavelengths spaced more or less evenly across the spectral range. Figures 1 through 9 are reproductions of scanner tracings of the stars in this study. The wavelengths chosen are those listed in Tables I or II and are marked on these tracings; they were selected so they lie in spectral regions containing absorption lines with equivalent widths no greater than 0.1A for most spectral types. The first entry in Table II is the absolute calibration of αLyrae as given by Code (1959).

Table II also lists the monochromatic magnitudes $\Delta M(\frac{1}{\lambda})$, of the stars used in this study. The definition of $\Delta M(\frac{1}{\lambda})$ is

$$(11) \qquad \Delta M(\tfrac{1}{\lambda}) = -2.5 \log \left[F_\nu(\lambda)/F_\nu(5560A) \right] ,$$

where $F_\nu(\lambda)$ is the monochromatic flux per unit frequency interval averaged over a roughly 15A band width centered at λ.

These results have been compiled in the manner indicated above from the observations made primarily at the 60-inch and 100-inch telescopes by Code and by the author. It is somewhat difficult to ascribe a measure of precision to these observations since this depends on the spectral region, the spectral type and magnitude of the star, declination, etc. Successive observations yield a typical probable error in monochromatic magnitudes at 3400A due to random errors only of 0.04. This, of course, diminishes for increasing wavelengths since the physical complications become less and the sensitivity of $\Delta M(\frac{1}{\lambda})$ diminishes as 5560A is approached. On the other hand, αLyrae, being very bright and possessing a smooth energy distribution outside the Balmer region, yields scanner deflections whose probable errors are less than 1% of the deflections in the blue and visual regions and around 2% in the 3400A - 3650A region. Being a small quantity, a 1% error in deflection produces nearly a 0.01 error in monochromatic magnitude. The observations giving the most difficulty are the late-type stars whose abundance of absorption lines gives rise to extremely jagged scanner tracings. This

Table II

MONOCHROMATIC MAGNITUDES, $\Delta M(\frac{1}{\lambda})$

$\lambda(\mu)$	0.340	.365	.386	.404	.419	.459	.506	.556
$1/\lambda$	2.94	2.74	2.59	2.48	2.39	2.18	1.975	1.80
α Lyr	+1.14	+1.04	-0.07	-0.19	-0.18	-0.14	-0.07	0.00
β Ari	1.38	1.22	0.25	0.02	-0.02	-0.06	-0.01	0.00
σ Boo	1.39	1.20	0.57	0.43	0.35	0.19	0.10	0.00
π^3 Ori	1.46	1.22	0.79	0.50	0.42	0.22	0.10	0.00
110 Herc.	1.40	1.24	0.77	0.56	0.47	0.25	0.11	0.00
β Com.	1.58	1.34	1.23	0.74	0.65	0.32	0.18	0.00
51 Peg.	1.74	1.50	1.13	0.91	0.80	0.37	0.18	0.00
HD140283	1.36	1.09	0.76	0.65	0.56	0.32	0.16	0.00
HD19445	1.30	1.08	0.74	0.55	0.49	0.26	0.13	0.00

$\lambda(\mu)$	.581	.605	.667	.746	.800	.875	.909	1.000
$1/\lambda$	1.72	1.65	1.50	1.34	1.25	1.14	1.09	1.00
α Lyr	+0.06	0.10	0.22	0.35	0.46	0.48	0.51	0.56
β Ari	0.04	0.09	0.19	0.30	0.37	0.41	0.38	0.40
σ Boo	-0.03	-0.04	-0.06	-0.07	-0.07			
π^3 Ori	-0.03	-0.04	-0.08	-0.11	-0.06	-0.01	-0.03	-0.04
110 Herc.	-0.04	-0.05	-0.10	-0.14				
β Com.	-0.04	-0.09	-0.14	-0.15	-0.21	-0.12	-0.15	-0.28
51 Peg.	-0.07	-0.16	-0.19	-0.21	-0.19	-0.08	-0.24	-0.34
HD140283	-0.05	-0.10	-0.23	-0.34				
HD19445	-0.06							

may be readily seen by comparing Figures 1 and 7 which are scanner tracings of αLyrae and 51 Peg, respectively.

It should be pointed out that the numbers in the above table or the solid curves drawn from them in Figures 11 through 19 tell only half the story for late-type stars. One must know to what point along the deflection axis of the scanner tracing the listed monochromatic magnitude corresponds. It is obvious in a late-type star there is considerable ambiguity concerning this point as will be seen by again inspecting Figure 7 in the blue and ultraviolet regions. The equipment and seeing noise somewhat complicate this problem further. One should present a scanner tracing to accompany each set of monochromatic magnitudes indicating at each wavelength where there is doubt ~~of~~ the point at which the reduction is made. In this study there is a quite definite way in which the points were reduced. Since these monochromatic magnitudes are eventually to be compensated for any line absorption existing in the corresponding band pass in order to obtain the continuum, an average of the deflection in a roughly 15A interval was taken. In most cases this would seem trivial, but some of the wavelength points in late-type stars are situated where the deflection is quite sensitive to wavelength changes because of the extreme unevenness of the tracings. The results in Table II as well as the figures will be discussed further in chapter 4 and 5.

II. Measurement of Line Absorption

High dispersion spectra were obtained with the 100-inch coude spectrograph in order to measure the line blanketing coefficient in the 15A band pass centered about the wavelengths indicated in the previous section. These spectra were generally obtained with the 32-inch camera giving a dispersion of 10A/mm and 15A/mm in the blue and visual regions, respectively. The 72-inch and 114-inch cameras were occasionally used in the blue regions particularly for the later types of stars where absorption line crowding becomes a problem. To obtain the ultraviolet on the same plate as the blue regions a mask was placed over the blue after the proper exposure time allowing only the ultraviolet region to receive an extended exposure. An additional iron arc spectrum slightly wider than the other comparison spectra was placed on the plate after the total stellar exposure to delineate the two regions. The emulsions used were the IIa-O in the blue regions and the 103a-D or 103a-F in the visual regions. For exposures requiring more than an hour the IIa-O plates were baked for 24 hours at 65 C. In order to convert emulsion density

Table III

STELLAR SPECTRA

HD	Name	Spectral Type	Plate Number	Emulsion	Cam.	Remarks
11636	β Ari	A5V	Ce. 11772	IIa-O	73"	
			11773	103a-F	73	
			12100	IIa-O	32	For U.V.
128167	σ Boo	F2V	11922	IIa-O	32	Observer: G. Wallerstein
30652	π^3 Ori	F6V	11627	IIa-O Bkd.	114	
			11768	103a-F	32	
			11829	IIa-O	32	
			11830	103a-D	32	
173667	110 Herc	F6V	12095	IIa-O	32	
114710	β Com	G0V	11780	IIa-O	73	
			11832	103a-D	73	
217014	51 Peg	G4V	12096	IIa-O	32	
			12099	103a-D	32	
140283			12101	IIa-O Bkd.	16	For U.V.
		F-Type	Pb. 3176	IIa-O Bkd.	72	Observer:
		Sub-	Pb. 3228	103a-F	72	J.L. Greenstein
		Dwarf				
19445		F-Type	Ce. 10788	IIa-O Bkd.	32	For U.V.
		Sub-	10784	IIa-O Bkd.	32	Observer:
		Dwarf	10849	IIa-D	32	E.M. Burbidge

or blackening to intensity the wedge spectrograph was used to obtain a "wedge" for every stellar spectra. This wedge was, of course, exposed and developed under the same conditions as the stellar plate in order to insure that the characteristic curve be the same for both plates. Primarily for the ultraviolet regions where the wedge does not extend and for back-up the step calibration strips were also used on most of the stellar plates. Table III gives the pertinent information about the plates obtained in this study.

The photometric reductions of these spectra were made with the Sinclair Smith microphotometer at the California Institute of Technology. The instrumentation has recently been equipped with a curve follower so that a signal from the photometer proportional to the transmission of a point on the photographic plate may be converted directly into intensity. A curve is drawn from the density deflections of the wedge plate or calibration strips in which, say, the x and y axes are proportional to the transmission and the intensity, respectively. This curve is drawn with conducting ink and placed in the curve follower where a high frequency current is passed through it generating a magnetic field. The curve follower possesses a seeking head which travels along the y axis centering itself over the curve. The input is the signal from the microphotometer which gives a proportional deflection along the x axis. A signal from the curve follower proportional to the y axis and therefore the intensity is amplified and recorded on tracing paper. An additional piece of equipment which may be used at this point is a current integrator for obtaining the area under the intensity deflection as a function of wavelength. The particular instrument used is still in the development stage and is not yet known for its reliability; however, when working properly it yields areas good to one percent as was verified by measuring the same areas manually with a planimeter. The value of such a device should be obvious both in the rapid measurements of the blanketing coefficients as well as the equivalent widths of unblended lines.

Because of the wide spectral range covered in these measurements one should draw a calibration curve for each band pass and for each plate used. By running a wedge at a particular wavelength on the microphotometer against a calibration curve drawn from the same wedge at the same wavelength one should obtain a straight line on the recorded tracing. The wavelength at which the wedge is photometered may be varied and the resulting departures

of the tracing give a measure of the change of the characteristic curve of the emulsion with wavelength and the intensity of the light producing this part of the spectrum. In this manner, it was found quite unnecessary to draw a calibration curve for each band pass. Unless one was dealing with over or under-exposed areas of the wedge the differences on the same plate across the sensitivity range used were no more than one or two percent of the local deflection. Moreover, similar results followed for the difference between two different plates provided they were the same emulsion with the same shipment number and were of comparable exposure times. (All the plates were developed in the rather standard way using D-19 developer for 4 minutes at 68°F, etc.) Similarly, in the ultraviolet the differences between strip calibrations under the above qualifications were negligible. These results allowed for a considerable reduction of the calibration curves required from perhaps a hundred to around ten. It has been suggested in the future a family or catalog of calibration curves be constructed covering the range of shapes generally occuring in practice. One could quickly select that curve best matching any particular wedge.

It should be pointed out that the photometric errors involved in placing the continuum or the clear region at their correct deflections do not affect the blanketing coefficient measures nearly as severely as the equivalent widths of lines. The blanketing coefficient γ, defined by

$$\gamma = \int_{\lambda_0 - 7.5A}^{\lambda_0 + 7.5A} F_\lambda \, d\lambda \Big/ \int_{\lambda_0 - 7.5A}^{\lambda_0 + 7.5A} F_c \, d\lambda \,, \tag{12}$$

is clearly a measure of the percentage of the continuum flux which is emitted in this 15A band pass. Except for later-type stars in the ultraviolet γ is generally greater than 80%. On the other hand, the equivalent width W, of the lines in this 15A band pass is related to γ by

$$W/15A = 1 - \gamma \,, \tag{13}$$

indicating that W percentage-wise is generally much more sensitive to these errors than γ. Table IV gives the values of γ as defined above for the stars in this study obtained from the plates listed in Table III.

Table IV

BLANKETING COEFFICIENT

Star \ λ	3400	3650	3860	4040	4190	4590	5060	5560	5810	6050
β Ari	0.92	0.95	0.91	0.97	0.96	0.96	>0.99	>0.99	>0.99	>0.99
σ Boo		0.81	0.88	0.90	0.93	0.94				
π^3 Ori(1)	0.75*	0.76*	0.83	0.86	0.84	0.90	0.95	0.98	0.99	>0.99
π^3 Ori(2)		0.76*	0.83	0.87		0.90	0.95	0.98	0.99	>0.99
110 Herc.	0.79*	0.74*	0.81	0.85	0.86	0.92				
β Com.	0.74*	0.65*	0.53*	0.77*	0.75*	0.87	0.93	0.97	0.97	0.99
51 Peg.	0.66*	0.69*	0.59*	0.75*	0.75*	0.85	0.92	0.95	0.96	0.99
HD19445	0.89	0.92	0.94	0.96	0.98	>0.99	>0.99	>0.99	>0.99	>0.99
HD140283	0.96	0.96	0.96	>0.99	>0.99	>0.99	>0.99	>0.99	>0.99	>0.99
Sun	0.74*	0.65*	0.53*	0.76	0.74	0.88	0.93	0.97	0.98	>0.99

The entry π^3 Ori(1) is the result of measures of the plates Cell627 and Cell768. These measurements were completely independent of those made with the plates Cell829 and Cell830 and therefore give an estimate of the precision of the results. The probable error due to random errors of measurement appears to be less than 0.01. The starred entries are upper values since it is suspected that overlapping absorption lines have suppressed the continuum in these regions. The values for β Com at λ3400, λ3650 and λ3860 have been taken from the Utrecht Atlas (1940) since none of the available plates extends to this region. In the blue and visual regions the blanketing coefficients of β Com are nearly identical with those for the center of the solar disk taken from the atlas; the values in the ultraviolet should therefore be reliable to a few percent. The atlas was also used to obtain the blanketing coefficients for the Sun, the results of which will be used in Chapter 5. The blanketing values for HD19445 and the blue and visual regions of HD140283 were taken from tracings of Cel0784, Cel0788 and Cel0849, and Pb. 3176 and Pb. 3228 kindly supplied to the writer by A. R. Sandage and J. L. Greenstein, respectively. In Chapter 4 these blanketing measures are applied to the observed monochromatic fluxes.

Fig.1

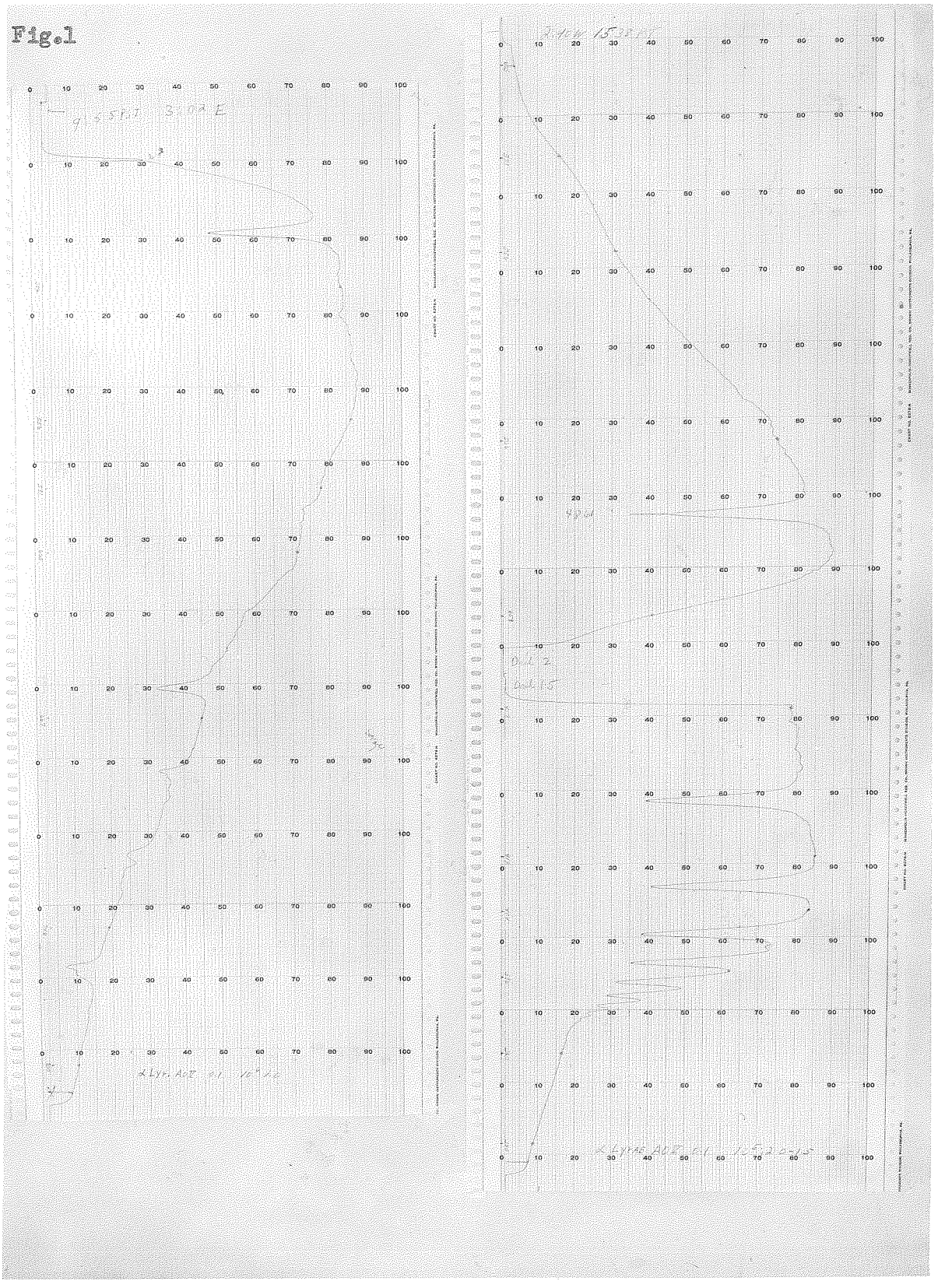

Fig.2

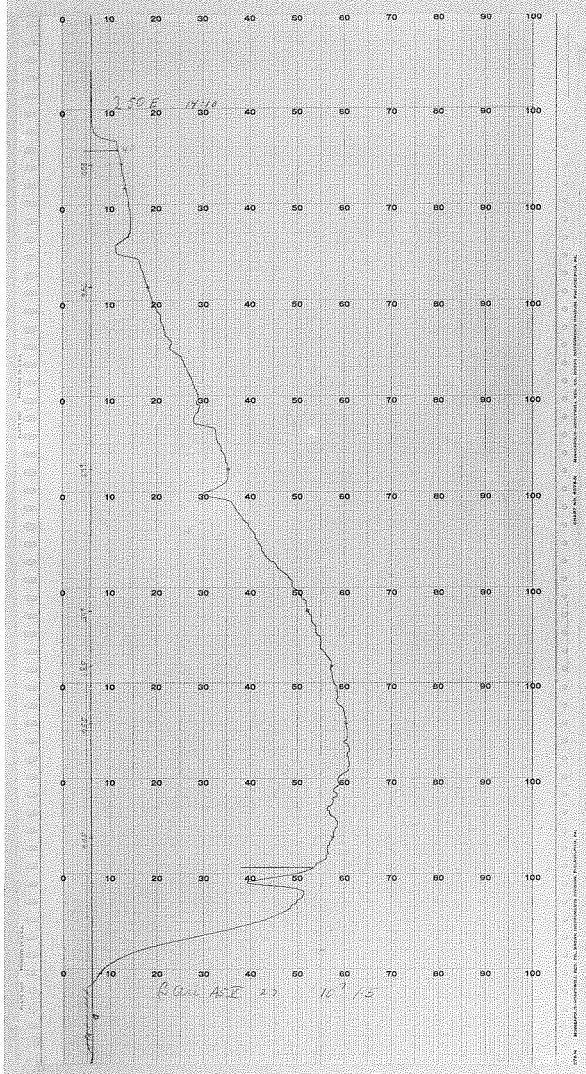

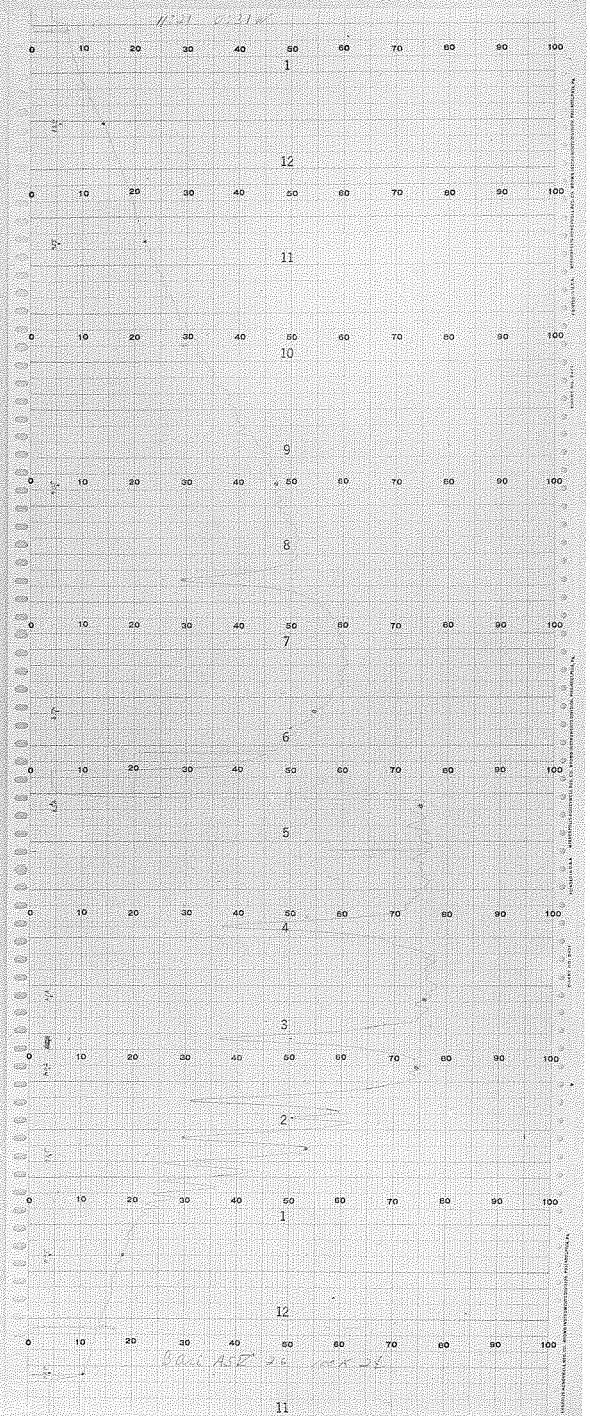

Fig.3

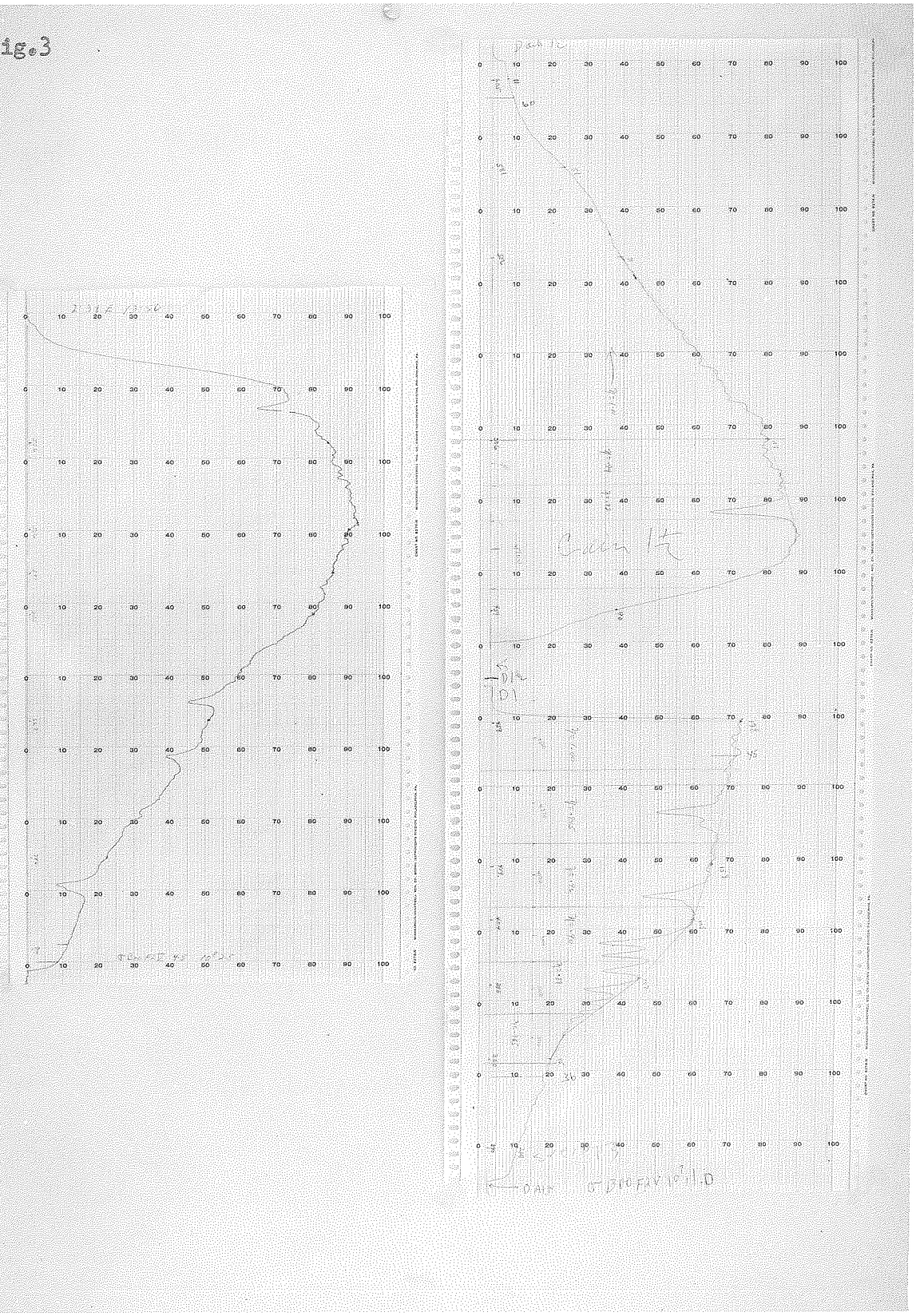

Fig.4

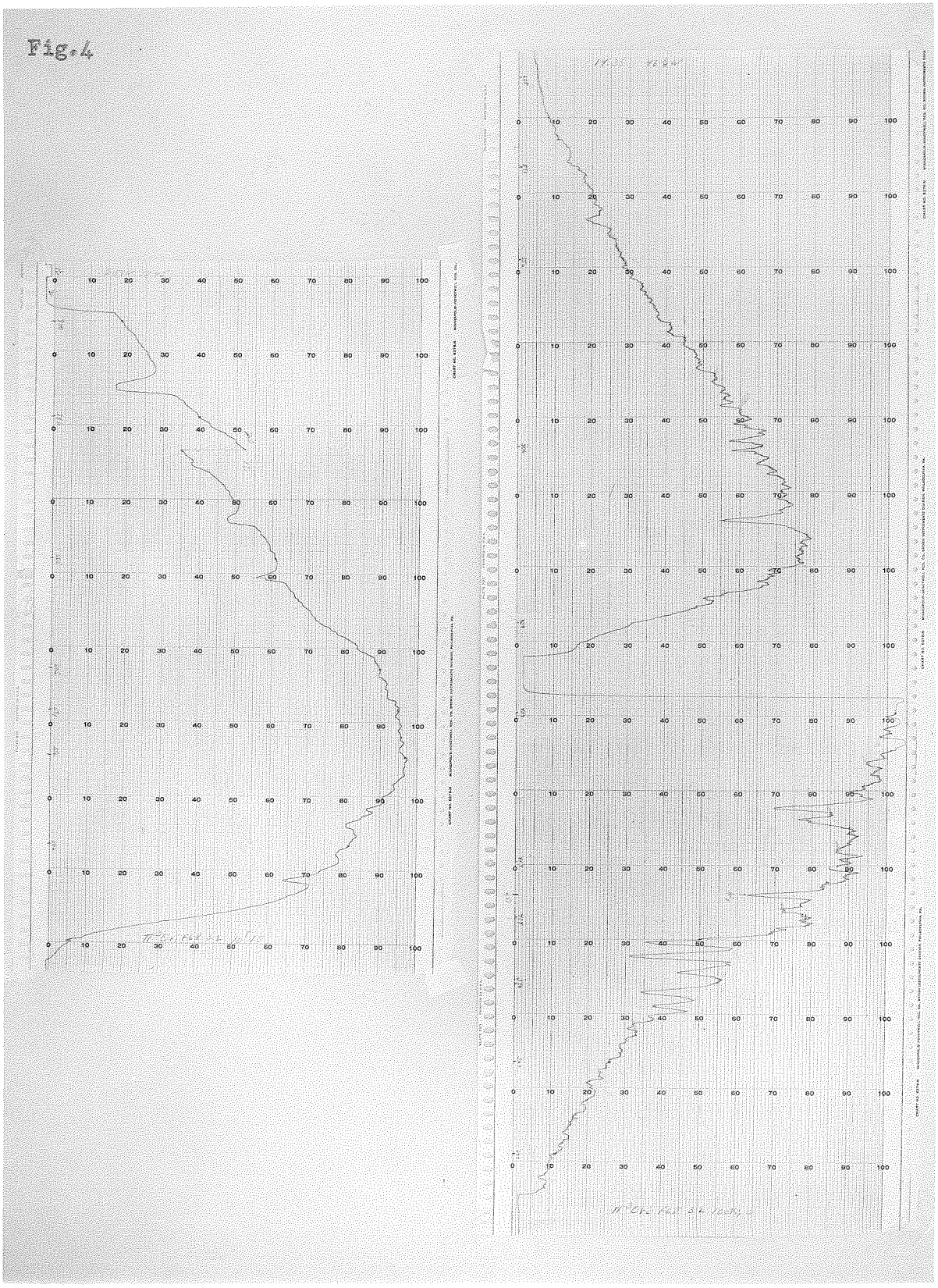

Fig.5

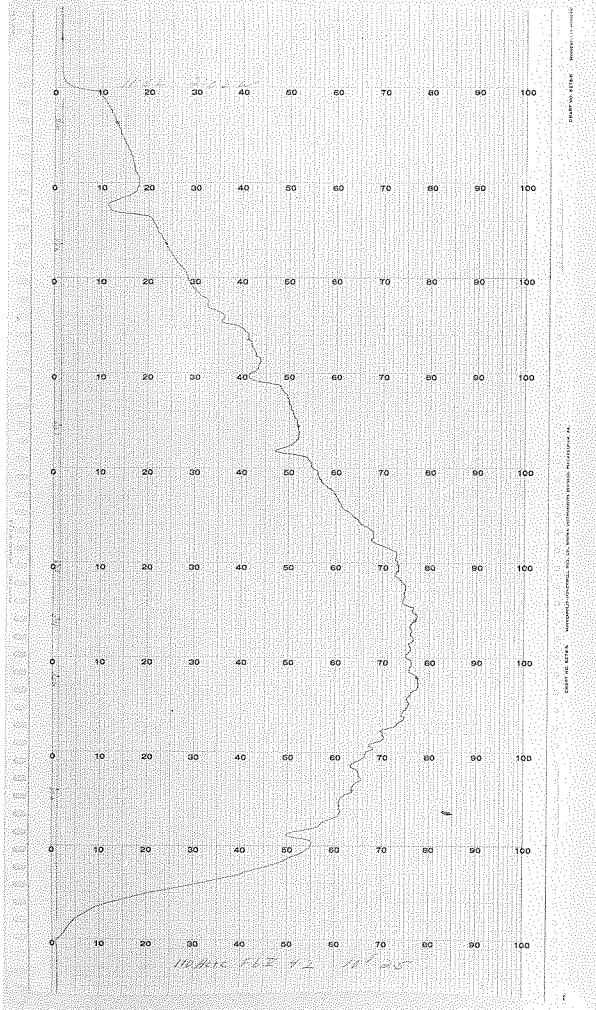
0 10 20 30 40 50 60 70 80 90 100
110 MHz FIELD #2

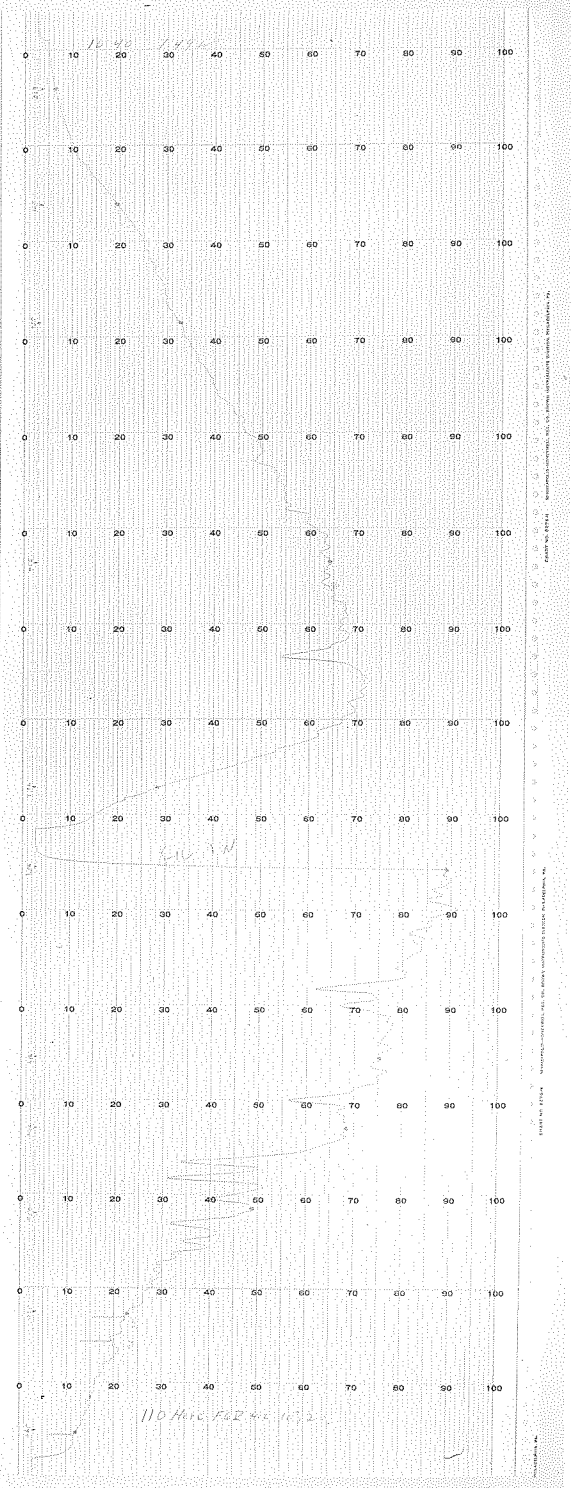
0 10 20 30 40 50 60 70 80 90 100
110 MHz FIELD #2

Fig.6

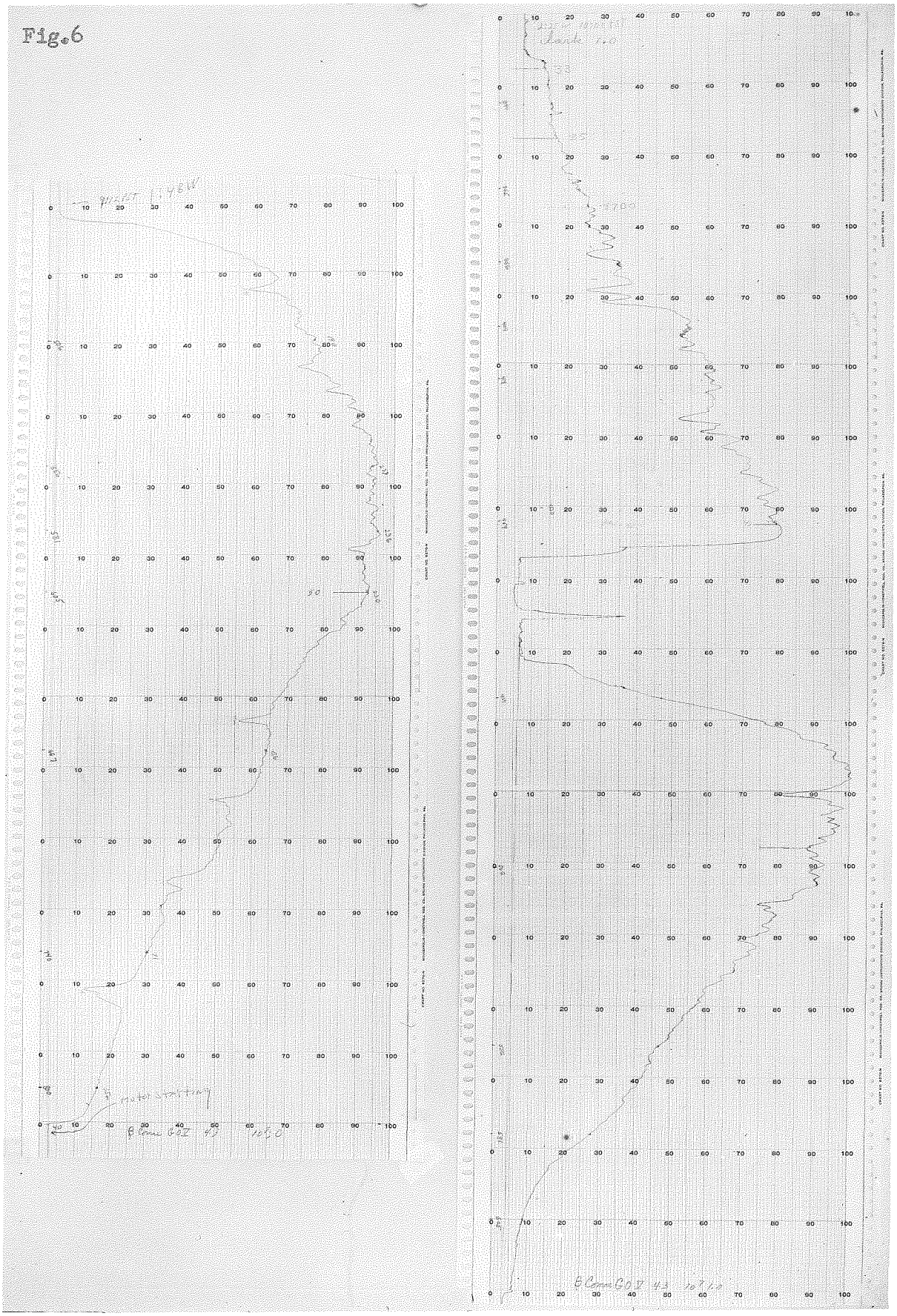

Fig.7

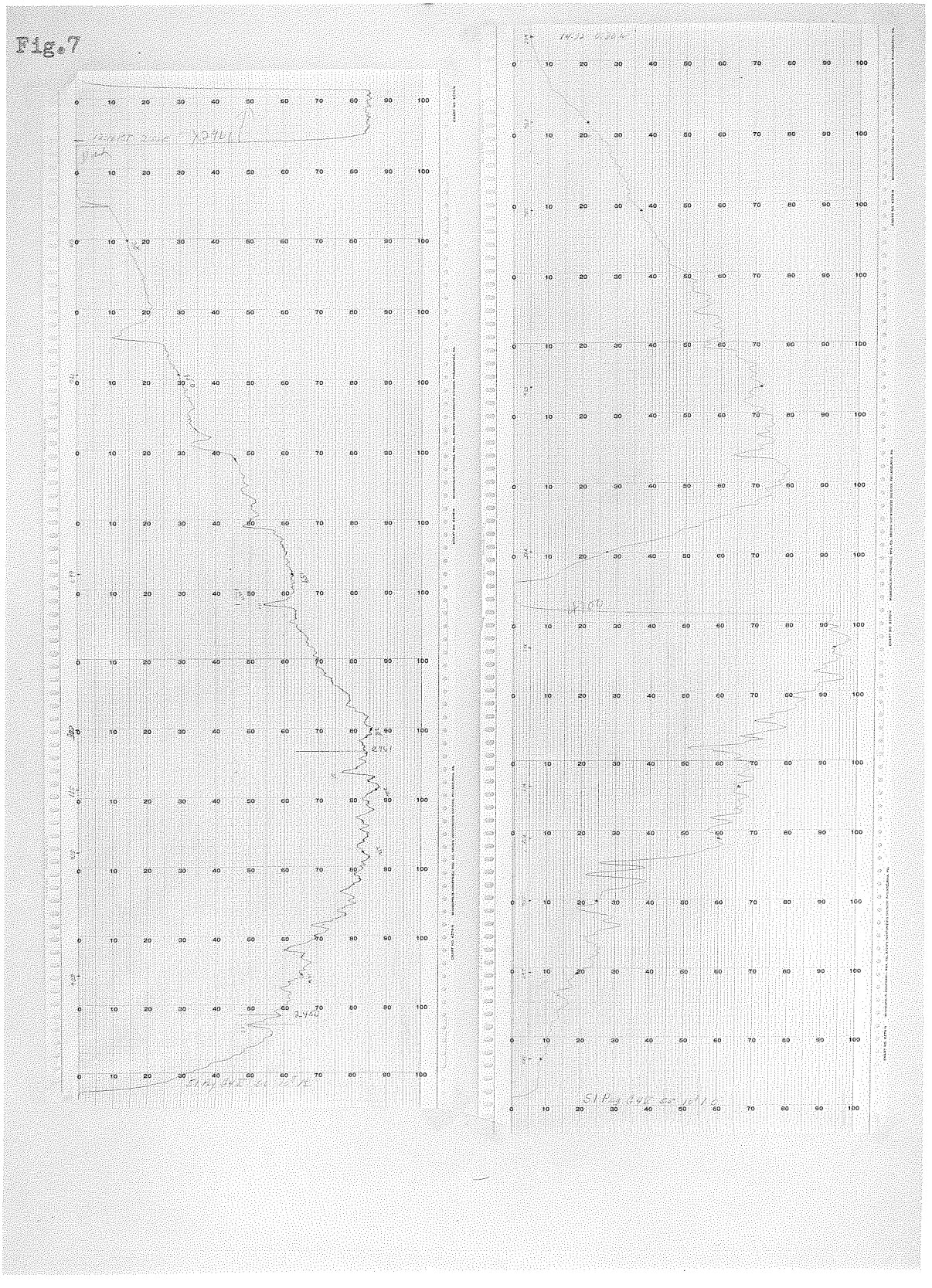

Fig.8

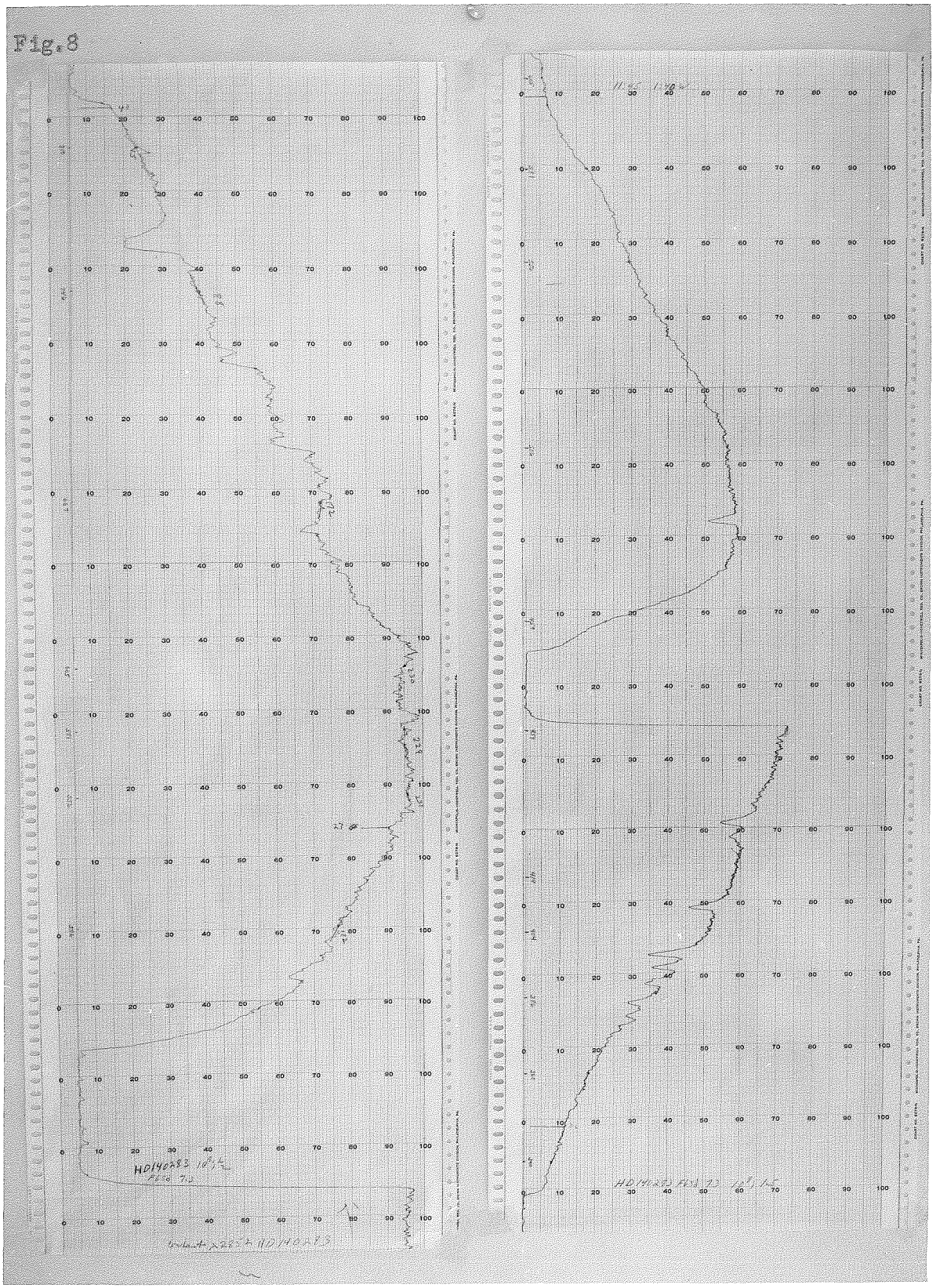

Fig.9

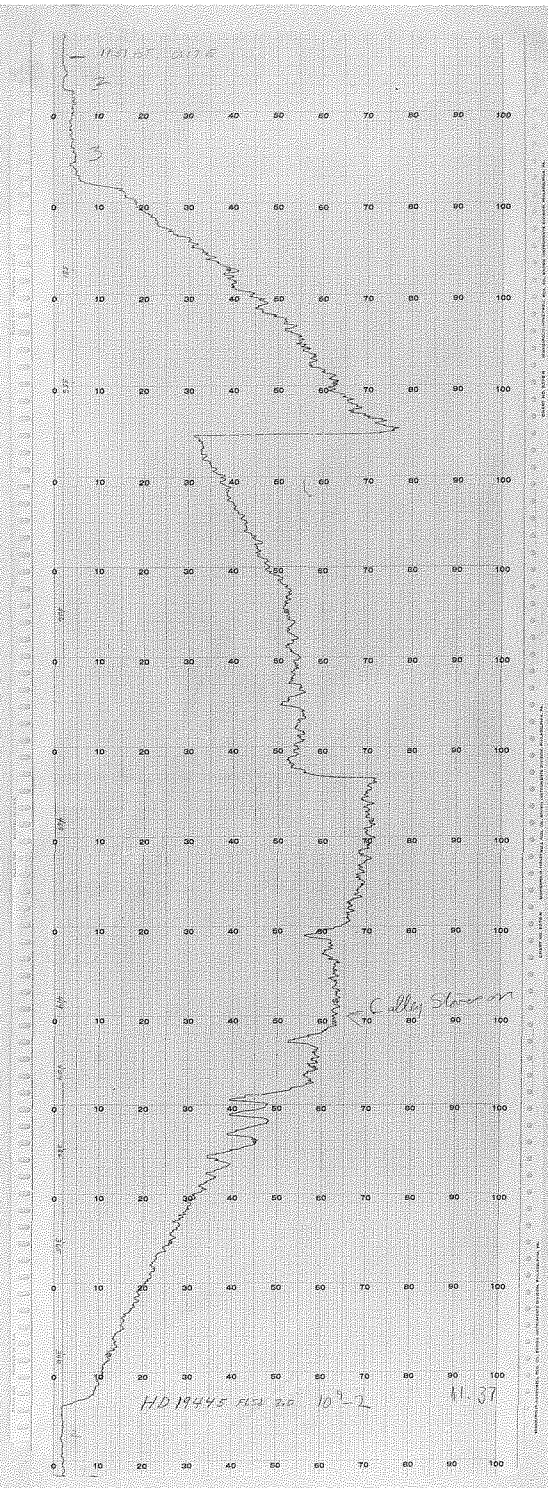

III. MODEL ATMOSPHERE COMPUTATIONS

The primary purpose for constructing the following models is to obtain the continuous monochromatic flux emerging from the surface of the stellar atmospheres in order to compare them with the observations. The qualifications under which these models were constructed are stated in the introduction. These atmospheres are completely specified by the effective temperature since the other parameters — the surface gravity g, and the relative abundance of the elements, are adjusted to coincide with main-sequence stars. In particular, the hydrogen to metals ratio A, is taken as log A = 3.8 and log g, which is essentially constant, ranges from 4.44 to 4.39 corresponding to a distribution of effective temperatures from 5500° to 7000°K. These atmospheres were taken to be in hydrostatic equilibrium. The temperature distribution for a grey atmosphere in radiative equilibrium was used, namely

$$T^4 = \frac{3}{4} T_e^4 \left[\tau + q(\tau) \right] \quad , \tag{14}$$

where $q(\tau)$ comes from the exact solution to the grey atmosphere problem by Mark (1947) and is conveniently tabulated by Woolley and Stibbs (1953). The relation for an atmosphere in hydrostatic equilibrium is

$$\frac{dp}{d\tau} = g/\bar{k} \quad , \tag{15}$$

where p, τ and $\bar{k}$ are the pressure, optical depth and mean opacity, respectively. In this case, $\bar{k}$ is the Rosseland mean opacity and depends on the temperature and electron pressure p_e. Since the chemical composition is specified the electron pressure may be tabulated as a function of temperature and pressure, and in this way $\bar{k}$ may be found as a function of temperature and pressure. A tabulation of log p_e against log p and θ ($\theta = 5040°/T$) was given by Strömgren (1944) for log A = 3.8 using a relative abundance of the metals found by Goldschmidt (1937). Since the ionization potentials among the various metals significantly contributing to the electron pressure differ little, the electron pressure is not sensitive to changes in the relative abundances of the metals among themselves. Strömgren (unpublished) has also

compiled a table of $\overline{k}$ due to neutral hydrogen and the negative ion as a function of θ and log P_e. These tables were used to numerically integrate equation 15.

In order to begin the integrations the following starting procedure was used. A small value of p_e is adopted. With this value and the boundary temperature the corresponding values of p and $\overline{k}$ are found from the tables which yield an approximate value for τ_0 through equation 15. If τ_0 is still so small that the temperature has not significantly changed, the choice of p_e was appropriate and one now has a suitable set of starting values. It should be noted that the error introduced in this procedure will be a negligible percentage of the values in the principle part of the atmosphere where τ, p and p_e are several orders of magnitude greater. Selecting an intergration interval $\Delta\tau$ one obtains the first estimate of the pressure, $p_1^{(1)}$, at the new optical depth $\tau_1 = \tau_0 + \Delta\tau$ by the relation

$$p_1^{(1)} = p_0 + \left.\frac{dp}{d\tau}\right|_1 \cdot \Delta\tau \,, \tag{16}$$

where $dp/d\tau|_1$ is evaluated at τ_0. Next, $\frac{1}{2}(p + p_0)$ is calculated and a temperature half way between $\theta(\tau_0)$ and $\theta(\tau_1)$ is picked. With these values one obtains a new estimate of the pressure gradient $\left.\frac{dp}{d\tau}\right|_2$ and computes

$$p_1^{(2)} = p_0 + \left.\frac{dp}{d\tau}\right|_2 \cdot \Delta\tau \,. \tag{17}$$

This is continued to the nth stage where $p_1^{(n)}$ becomes stationary. With this p_1 and $\theta(\tau_1)$, $p_e(\tau_1)$ and $\overline{k}(\tau_1)$ are obtained which become the final values. In this manner the iterative process is extended to successive intervals of optical depth. By astutely picking the trial pressure gradient one may reach a stationary value of p on the first or second iteration. The run of the variables p, p_e, $\overline{k}$, θ and τ through the stellar atmosphere was obtained and the results are shown in Table V.

Although τ is the running parameter in these calculations, the important relationship for flux computations is that between the temperature and the pressure (or electron pressure). Strongren (unpublished) has also compiled tables of $k_\lambda/\overline{k}$ as a function of θ and log p_e for various wavelengths

Table V

MODEL ATMOSPHERES

$T_e = 5500^{\circ}K$; log g = 4.44					$T_e = 5800^{\circ}K$; log g = 4.44			
τ	Θ	log p	log p_e	log $\bar{k}$	Θ	log p	log p_e	log $\bar{k}$
0.00	1.131				1.072			
0.01	1.122	3.92	0.02	-1.13	1.068	3.89	0.01	-1.22
0.02	1.114	4.05	0.12	-1.04	1.055	4.07	0.18	-1.07
0.03	1.109	4.14	0.17	-0.99	1.050	4.17	0.26	-1.00
0.04	1.102	4.21	0.23	-0.95	1.042	4.24	0.33	-0.94
0.06	1.089	4.31	0.32	-0.88	1.031	4.34	0.42	-0.87
0.08	1.079	4.38	0.38	-0.83	1.021	4.40	0.50	-0.80
0.10	1.070	4.44	0.43	-0.80	1.011	4.45	0.56	-0.77
0.12	1.061	4.48	0.49	-0.75	1.003	4.50	0.61	-0.74
0.14	1.052	4.51	0.53	-0.73	0.996	4.54	0.65	-0.70
0.16	1.046	4.55	0.57	-0.70	0.990	4.57	0.69	-0.67
0.20	1.030	4.62	0.65	-0.64	0.975	4.62	0.77	-0.63
0.24	1.018	4.66	0.71	-0.60	0.965	4.67	0.82	-0.59
0.28	1.005	4.68	0.76	-0.58	0.955	4.70	0.89	-0.56
0.32	0.994	4.70	0.80	-0.56	0.940	4.74	0.92	-0.54
0.36	0.983	4.72	0.84	-0.54	0.935	4.76	0.94	-0.52
0.40	0.972	4.75	0.88	-0.52	0.920	4.79	1.01	-0.50
0.50	0.949	4.83	0.98	-0.46	0.900	4.84	1.10	-0.44
0.60	0.928	4.89	1.06	-0.42	0.880	4.88	1.20	-0.40
0.70	0.911	4.92	1.13	-0.39	0.863	4.92	1.30	-0.32
0.80	0.894	4.95	1.20	-0.35	0.847	4.94	1.38	-0.26
0.90	0.878	4.98	1.28	-0.29	0.833	4.97	1.47	-0.19
1.00	0.866	5.00	1.34	-0.26	0.820	4.99	1.55	-0.14
1.20	0.842	5.04	1.48	-0.18	0.798	5.02	1.70	-0.04
1.40	0.818	5.06	1.62	-0.08	0.777	5.04	1.85	+0.07
1.60	0.790	5.08	1.79	+0.02	0.760	5.05	1.97	0.15
2.00	0.770	5.10	1.93	0.12	0.730	5.08	2.18	0.31
2.50	0.740	5.11	2.13	0.27	0.700	5.10	2.41	0.49
3.00	0.713	5.12	2.33	0.43	0.678	5.12	2.58	0.62

Table V (Cont.)

MODEL ATMOSPHERES

T_e = 6100 k; log g = 4.43					T_e = 6400 k; log g = 4.42			
τ	Θ	log p	log p_e	log $\bar{k}$	Θ	log p	log p_e	log $\bar{k}$
0.00	1.020				0.971			
0.01	1.013	3.80	0.00	-1.31	0.965	3.87	0.17	-1.22
0.02	1.005	4.09	0.27	-1.07	0.960	4.05	0.31	-1.10
0.03	0.999	4.18	0.34	-1.00	0.953	4.15	0.41	-1.01
0.04	0.990	4.25	0.42	-0.94	0.949	4.22	0.49	-0.94
0.06	0.982	4.35	0.52	-0.86	0.938	4.32	0.58	-0.87
0.08	0.974	4.41	0.58	-0.80	0.930	4.39	0.66	-0.80
0.10	0.965	4.46	0.64	-0.77	0.920	4.44	0.73	-0.76
0.12	0.958	4.51	0.69	-0.73	0.913	4.49	0.80	-0.70
0.14	0.949	4.54	0.74	-0.70	0.907	4.52	0.84	-0.67
0.16	0.942	4.58	0.79	-0.67	0.899	4.55	0.89	-0.64
0.18	0.935	4.61	0.83	-0.64	0.891	4.58	0.95	-0.60
0.20	0.928	4.63	0.89	-0.59	0.885	4.60	0.98	-0.58
0.24	0.917	4.68	0.93	-0.57	0.869	4.64	1.07	-0.52
0.28	0.906	4.71	1.00	-0.52	0.862	4.67	1.14	-0.47
0.32	0.896	4.74	1.03	-0.51	0.851	4.70	1.21	-0.41
0.36	0.885	4.77	1.07	-0.49	0.840	4.72	1.28	-0.37
0.40	0.877	4.80	1.15	-0.42	0.833	4.74	1.33	-0.33
0.50	0.855	4.84	1.28	-0.33	0.812	4.78	1.47	-0.23
0.60	0.836	4.87	1.39	-0.27	0.795	4.81	1.60	-0.13
0.70	0.820	4.90	1.50	-0.20	0.780	4.83	1.72	-0.05
0.80	0.805	4.92	1.60	-0.12	0.765	4.85	1.81	+0.01
0.90	0.792	4.94	1.70	-0.05	0.754	4.86	1.90	0.09
1.00	0.780	4.95	1.79	+0.01	0.742	4.87	2.00	0.16
1.20	0.759	4.98	1.94	0.12	0.721	4.89	2.16	0.28
1.40	0.740	4.99	2.07	0.22	0.702	4.90	2.30	0.40
1.60	0.722	5.00	2.21	0.33	0.688	4.91	2.39	0.47
1.80	0.707	5.01	2.32	0.41	0.673	4.92	2.52	0.55
2.00	0.693	5.02	2.42	0.50	0.661	4.93	2.61	0.65
2.50	0.666	5.04	2.63	0.67	0.632	4.94	2.86	0.86
3.00	0.643	5.05	2.81	0.82	0.610	4.95	3.00	0.99
4.00	0.605	5.06	3.09	1.06	0.577	4.96	3.25	1.22

Table V (Cont.)

MODEL ATMOSPHERES

T_e = 7000 k; log g = 4.39

τ	Θ	log p	log p_e	log $\bar{k}$
0.00	0.889			
0.01	0.883	3.75	+0.44	-1.28
0.02	0.876	3.92	0.58	-0.98
0.03	0.870	4.02	0.68	-0.88
0.04	0.864	4.08	0.76	-0.83
0.06	0.855	4.18	0.85	-0.74
0.08	0.847	4.24	0.94	-0.67
0.10	0.840	4.29	1.02	-0.61
0.14	0.826	4.35	1.15	-0.51
0.18	0.814	4.41	1.26	-0.42
0.24	0.800	4.47	1.38	-0.33
0.30	0.785	4.51	1.50	-0.25
0.40	0.763	4.56	1.68	-0.10
0.50	0.745	4.59	1.82	+0.02
0.60	0.729	4.61	1.95	0.12
0.80	0.702	4.66	2.17	0.29
1.20	0.661	4.71	2.51	0.57
1.60	0.630	4.74	2.75	0.79
2.00	0.605	4.76	2.94	0.97
3.00	0.560	4.78	3.29	1.30

distributed across the spectrum. These enable one to compute the continuous monochromatic flux at the surface of a star through the relation

$$(18) \qquad F_\nu(0) = 2\int_0^\infty S_\nu(\tau_\nu)\cdot E_2(\tau_\nu)\, d\tau_\nu ,$$

where $S_\nu(\tau_\nu)$ is the source function and $E_2(\tau_\nu)$ is the second exponential integral function. Electron scattering is negligible for the range of temperatures considered in these models. The usual procedure of replacing the source function by the Planck function

$$(19) \qquad B_\nu(\tau_\nu) = \frac{2h\nu^3}{c^2}\left[e^{h\nu/kT(\tau)}-1\right]^{-1},$$

was followed here. The Planck function may be evaluated in terms of τ through equation 14. Moreover, through the relation

$$(20) \qquad \tau_\nu = \int_0^\tau \frac{k_\nu}{\bar{k}}\, d\tau ,$$

which may be numerically integrated with the aid of the corresponding model in Table V and Stromgren's tables, one may obtain an evaluation of the Planck function in terms of τ_ν for each wavelength. Although the emergent monochromatic flux may then be obtained through a numerical integration of equation 18, an approximate solution by a quadrature formula due to A. Reiz (Aller 1953) was generally used. The two-point approximation is

$$(21) \qquad F_\nu(0) = 0.884\, B_\nu(0.397) + 0.116\, B_\nu(2.723) .$$

At some of the wavelengths for different effective temperatures the ratio $k_\nu/\bar{k}$, is very nearly independent of optical depth. For these cases equation 18 may be evaluated exactly with $k_\nu/\bar{k}$ as a parameter. Chandrasekhar (1950) has tabulated the quantity $\mathcal{F}(\alpha,\beta)$ defined by

$$(22) \qquad F_\nu(0) = B_\nu(0)\,\mathcal{F}(\alpha,\beta) ,$$

where $\alpha = h\nu/kT$ and $\beta = k/\bar{k}$. The fluxes were also computed from these tables for those cases of constant $k_\nu/\bar{k}$. The differences between these two methods

were seldom greater than 3%. The latter values were adopted when the variation of $k_\nu/\overline{k}$ was sufficiently small that exact integration was considered more accurate. Moreover, two straight numerical integrations were performed at wavelengths where $k_\nu/\overline{k}$ varied significantly. The results agreed (perhaps fortuitously) with the two-point calculations to within 2%. It would seem that the one sigma errors in these flux values due solely to computations are less than 5% at the worst; furthermore, the relative fluxes (F_ν / F_ν (5560A)) should be considerably more accurate — probably 1 - 2% at the extreme.

Table VI lists F_ν at $\tau = 0$ for the above models. The last three rows are entries from model atmosphere computations by K. Osawa (1956) and S. Saito (1957). The T_e 7560 k and T_e 8900 k were found from interpolating between Osawa's log g = 4.0 and log g = 4.5 tables using log g = 4.35. Osawa's and Saito's models were constructed using the same ionization and opacity tables as was used in these calculations, so, all the models should be compatible. Osawa's models possess flux constancy through the atmosphere while Saito's model includes electron scattering.

In order to compare these fluxes with the observed relative fluxes F_ν(5560A) was interpolated from the entries and the monochromatic magnitudes $\Delta M(\frac{1}{\lambda})$ defined by equation 9 are listed in Table VII. Figure 10 is a graphical representation of these $\Delta M(\frac{1}{\lambda})$ values against $1/\lambda$.

Table VI

THEORETICAL SPECTRAL ENERGY DISTRIBUTIONS

$F_\lambda \times 10^5$ (ergs/sec.cm.^{2} $\Delta\lambda$)

T_e	λ2652 $\frac{1}{\lambda}$3.77	3647$^-$ 2.74$^+$	3647$^+$ 2.74$^-$	4235 2.36	5050 1.98	6250 1.60	8206$^-$ 1.22$^+$	8206$^+$ 1.22$^-$	9214 1.085	10503 0.953
5500°K	0.292	0.779	0.885	1.17	1.61	2.15	2.63		2.69	2.74
5800	0.416	1.03	1.25	1.64	2.13	2.66	3.13	3.13	3.18	3.19
6100	0.570	1.35	1.72	2.16	2.73	3.26	3.70	3.71	3.70	3.62
6400	0.745	1.69	2.35	2.82	3.46	3.97	4.31	4.33	4.23	4.09
7000	1.15	2.34	4.00	4.56	5.22	5.58	5.60	5.70	5.47	5.10
7560	1.53	2.73	5.95	6.33	6.78	6.85	6.40	6.70	6.31	5.82
8900	2.84	4.48	10.6	13.8	12.9	11.4	9.10	10.7	9.50	8.20
10700	6.71*	11.1	31.3	26.8	23.3	19.6	13.8	16.4		11.4

Table VII

THEORETICAL MONOCHROMATIC MAGNITUDES RELATIVE TO λ5560

T_e	λ2652 $\frac{1}{\lambda}$3.77	3647$^-$ 2.74$^+$	3647$^+$ 2.74$^-$	4235 2.36	5050 1.98	6250 1.60	8206$^-$ 1.22$^+$	8206$^+$ 1.22$^-$	9214 1.085	10503 0.953
5500°K	2.01	0.95	0.81	0.51	0.16	-0.15	-0.37		-0.40	-0.42
5800	1.90	0.92	0.70	0.42	0.13	-0.12	-0.29	-0.29	-0.31	-0.31
6100	1.80	0.87	0.60	0.36	0.10	-0.09	-0.23	-0.23	-0.23	-0.20
6400	1.75	0.86	0.50	0.30	0.08	-0.07	-0.16	-0.17	-0.14	-0.10
7000	1.69	0.92	0.34	0.19	0.05	-0.03	-0.03	-0.05	0.00	+0.07
7560	1.63	1.00	0.16	0.09	0.02	0.00	+0.08	+0.02	+0.09	0.18
8900	1.58	1.09	-0.12	-0.13	-0.06	+0.08	0.32	0.14	0.27	0.43
10700	1.27*	0.72	-0.40	-0.24	-0.08	+0.10	0.48	0.30		0.69

* Evaluated at λ2279

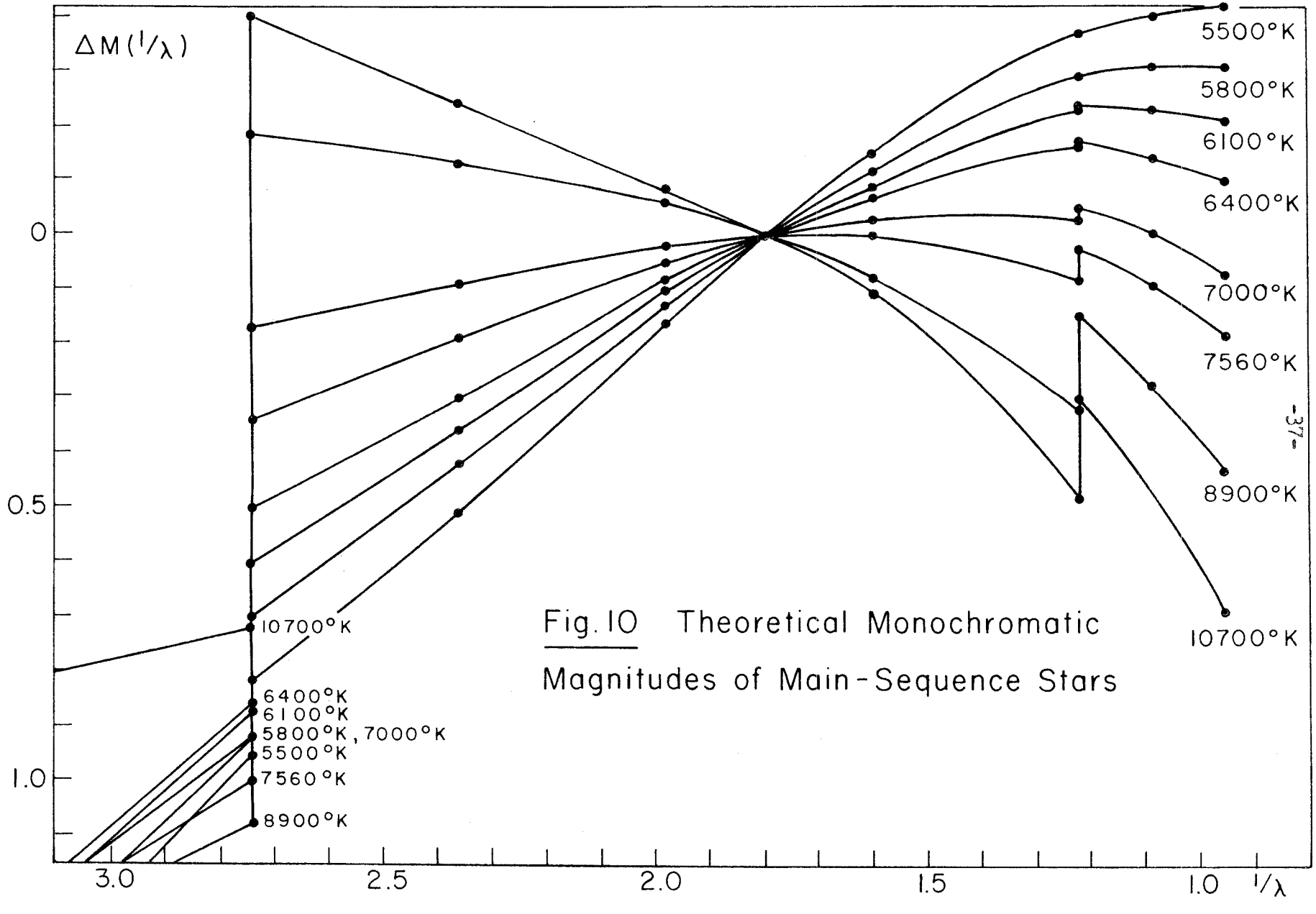

Fig. 10 Theoretical Monochromatic Magnitudes of Main-Sequence Stars

IV. COMPARISON OF THEORY AND OBSERVATIONS

It is now possible to compare the observed and theoretical energy curves. As was stated in the introduction, the scanner deflections in a particular wavelength interval are reduced by any line absorption existing in the region. The line absorption measurements listed in Table IV may be used to convert the observed deflections into line-free deflections. A curve defined by these converted points represents the energy distribution of the continuous flux of a star with an effective temperature in excess of the true temperature by an amount indicated in equation 1. Since the observations and calculations have been made relative to $\lambda 5560$, the blanketing coefficients should be on the same basis. Table VIII gives the relative blanketing coefficients in magnitudes defined by the relation

$$(23) \qquad \delta M = +2.5 \log \left[\gamma(\lambda) \,/\, \gamma(5560) \right] \quad .$$

These values algebraically subtracted from the monochromatic magnitudes obtained with the scanner and listed in Table II give the line-free values.

Table VIII

RELATIVE BLANKETING COEFFICIENTS, δM

λ	3400	3650	3860	4040	4190	4590	5060	5560	5810	6050
Star										
β Ari	0.09	0.05	0.10	0.03	0.04	0.04	0.00	0.00	0.00	0.00
γ Boo		0.23	0.13	0.11	0.08	0.07	0.02#	0.00	0.00	0.00
π^3 Ori	0.29	0.28	0.18	0.14	0.17	0.09	0.03	0.00	-0.01	-0.02
110 Herc.	0.24	0.31	0.21	0.16	0.15	0.07	0.03*	0.00	-0.01	-0.02
β Com.	0.27	0.44	0.66	0.25	0.28	0.12	0.05	0.00	-0.02	-0.03
51 Peg.	0.40	0.25	0.52	0.26	0.26	0.13	0.04	0.00	-0.01	-0.04
HD140283	0.04	0.04	0.04	0.00	0.00	0.00	0.00	0.00	0.00	0.00
HD19445	0.11	0.08	0.05	0.04	0.02	0.00	0.00	0.00	0.00	0.00

\# estimated from spectrum of α Can. Min. contained in Miltner-Williams Atlas (1946).

* the values for 110 Herc. and π^3 Ori for $\lambda > 5060$ are assumed to be the same.

Figures 11 through 19 illustrate the results graphically; the solid line is derived from the observed flux and the circled points are the blanketing compensated values. The dashed line corresponds to the model best fitting the

blanketing compensated distribution. The model for each case was obtained by interpolating in Figure 10 for an effective temperature yielding the best fit. The 'best fit' was decided to be that curve which agreed best with the red observations and to a lesser extent provided the best compromise in the visual and blue regions. For reasons to be described later no weight was ascribed to the spectral regions of $\lambda < 4000$, which evidently is consistently the region of least agreement.

Before discussing these results in more detail, one should perhaps comment on α Lyrae. Because so much is dependent on this star it was decided to include a plot of its flux distribution (Figure 11) and the model best fitting it. The metallic line absorption though practically non-existent was determined from a 100-inch Coude plate No. Cel2097 and the results are indicated in this figure. An effective temperature of 11,000° k which is compatible with the presently accepted value for an A0 V star seems to give the best agreement with the observed monochromatic flux.

It is apparent that the best agreement in the case of α Lyrae possesses several regions of marked disparity highlighted by the ultraviolet region shortward of λ3647, the ultraviolet and part of the blue region longward of λ3647 and the infrared past λ8206. At this stage one encounters the usual dilemma in attempting to decide what level of agreement between theory and observation is satisfactory, since, it is known the observations are of limited accuracy while on the other hand because of the a priori assumptions and approximations employed the models and the computations also possess a degree of uncertainty. It is of course difficult to place a one sigma confidence limit about the theoretical results and at the present time it is impossible to do the same for the ultraviolet calibration of α Lyrae since this region has been investigated only once — the Jungfraujoch measurements by Barbier and Chalonge (1940). The remainder of the spectral region has been subjected to two or three independent investigations (Code 1959); it seems certain that the monochromatic magnitudes relative to λ5560 compiled from these results are generally correct to within 0.1. However, it is clear that although the model agrees with the observations in a rough sense (that is, the model fits this spectral type better than any other) it almost surely does not yield the true values in the ultraviolet and blue regions irrespective of the observational error. The hypothesis that the α Lyrae

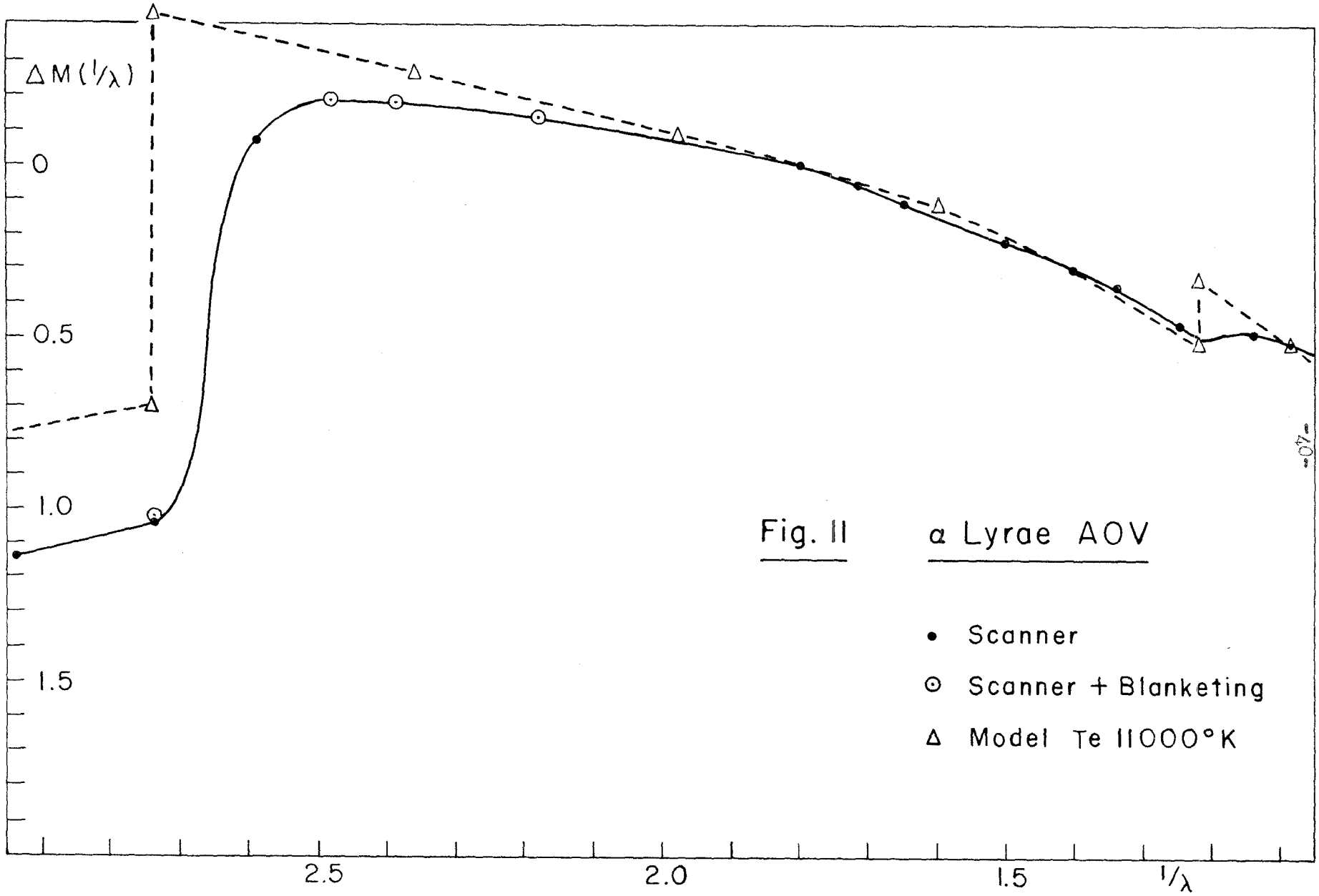
ΔM(1/λ)
0
0.5
1.0
1.5
2.5
2.0
1.5
1/λ
Fig. II
α Lyrae AOV
• Scanner
⊙ Scanner + Blanketing
Δ Model Te 11000°K

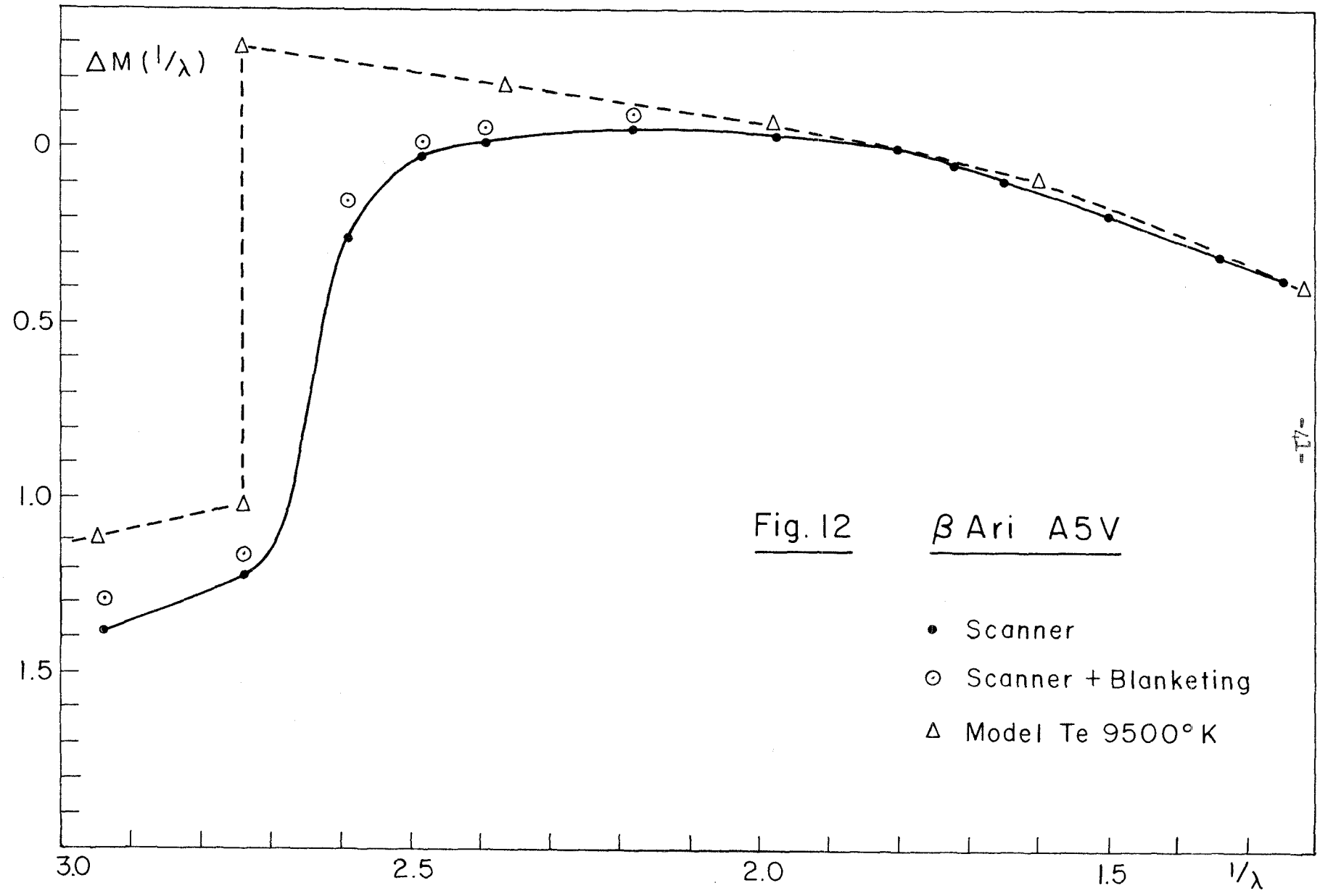
ΔM (1/λ)
0
0.5
1.0
1.5
3.0
2.5
2.0
1.5
1/λ
Fig. 12
β Ari A5V
Scanner
Scanner + Blanketing
Model Te 9500° K

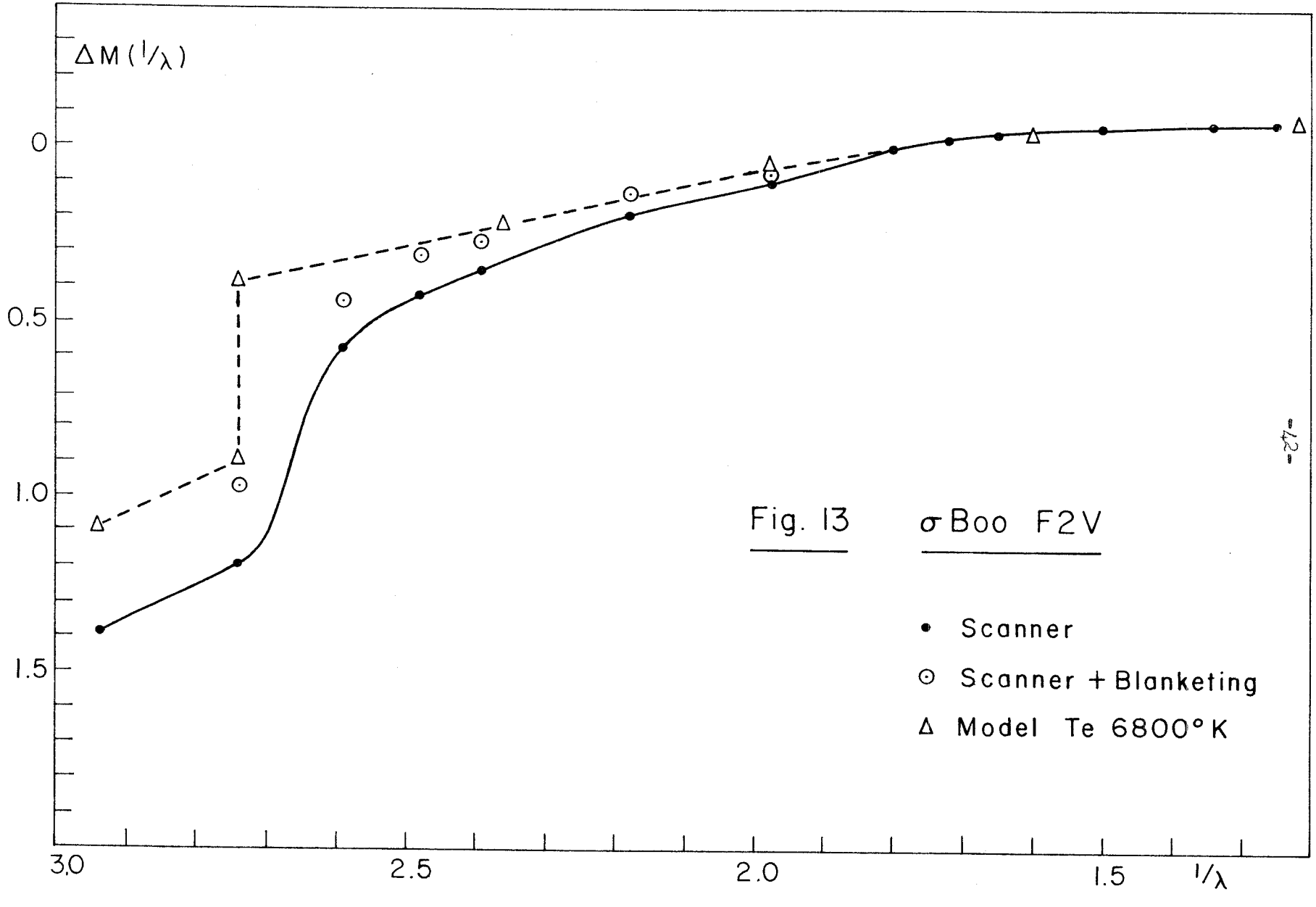
ΔM (1/λ)
0
0.5
1.0
1.5
3.0
2.5
2.0
1.5
1/λ
Fig. 13
σ Boo F2V
Scanner
Scanner + Blanketing
Model Te 6800° K

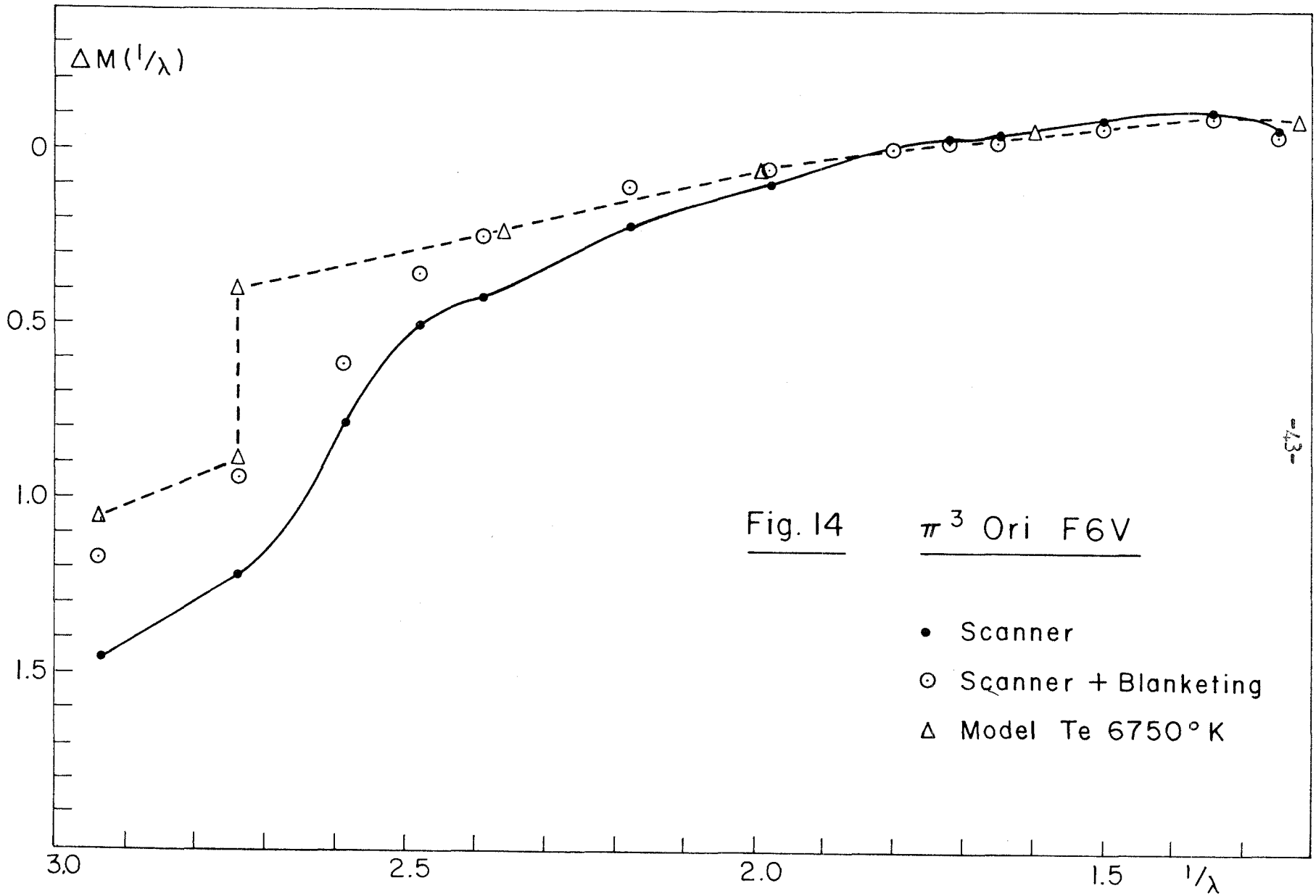
ΔM(1/λ)
0
0.5
1.0
1.5
3.0
2.5
2.0
1.5
1/λ
Fig. 14
π³ Ori F6V
Scanner
Scanner + Blanketing
Model Te 6750° K

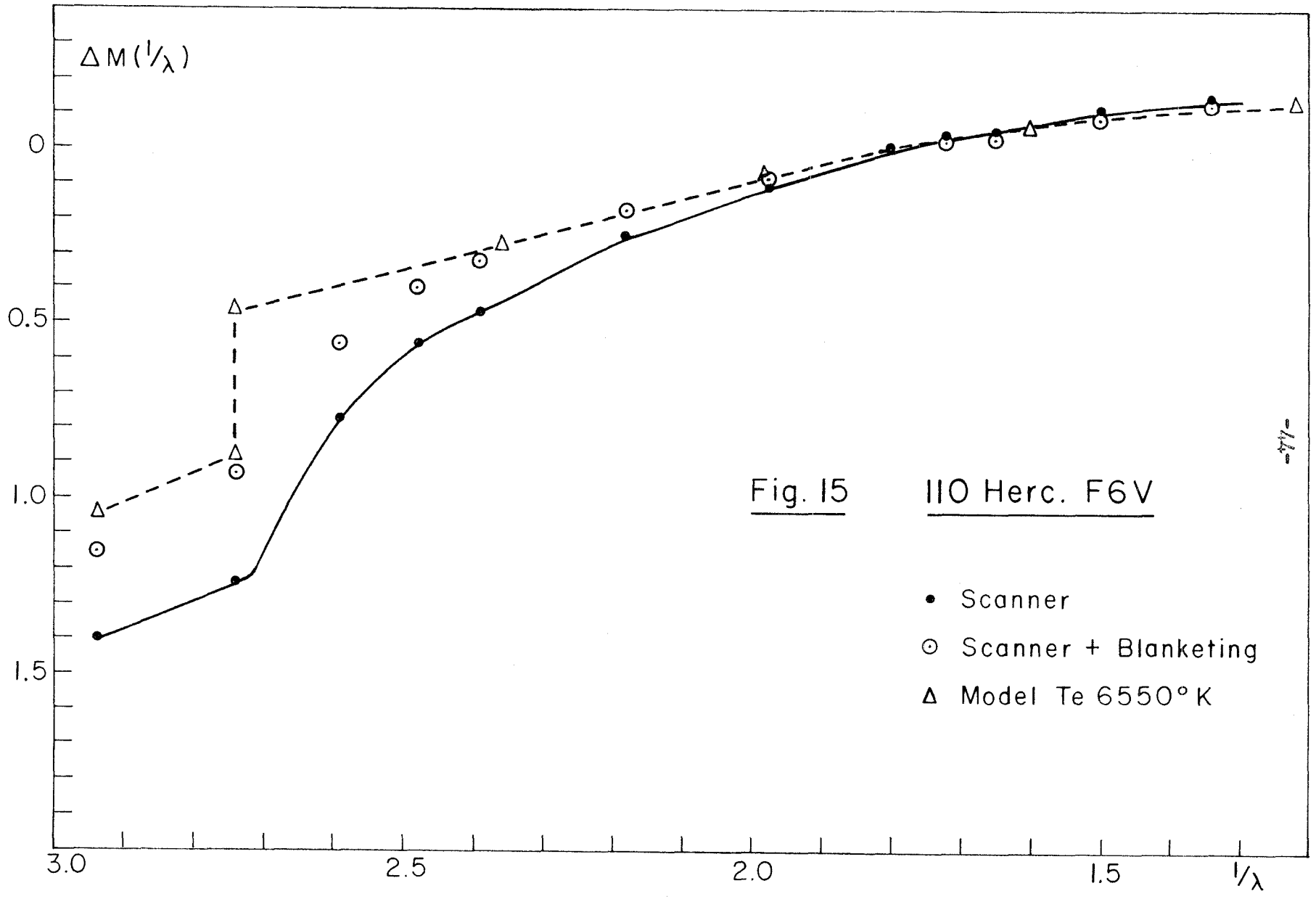
ΔM(1/λ)
0
0.5
1.0
1.5
3.0
2.5
2.0
1.5
1/λ
Fig. 15
110 Herc. F6V
Scanner
Scanner + Blanketing
Model Te 6550° K

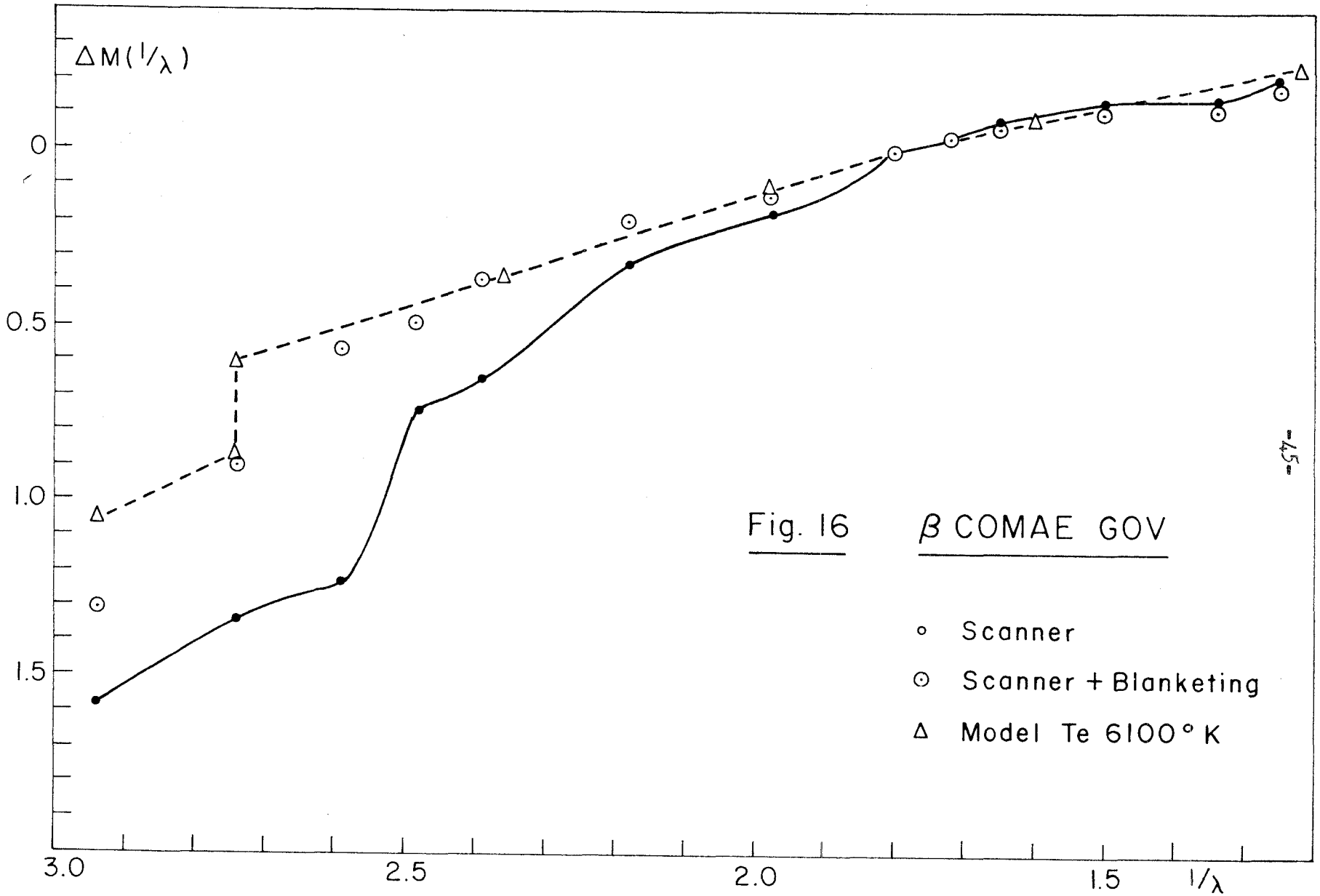
ΔM(1/λ)
0
0.5
1.0
1.5
3.0
2.5
2.0
1.5
1/λ
Fig. 16 β COMAE GOV
Scanner
Scanner + Blanketing
Model Te 6100° K

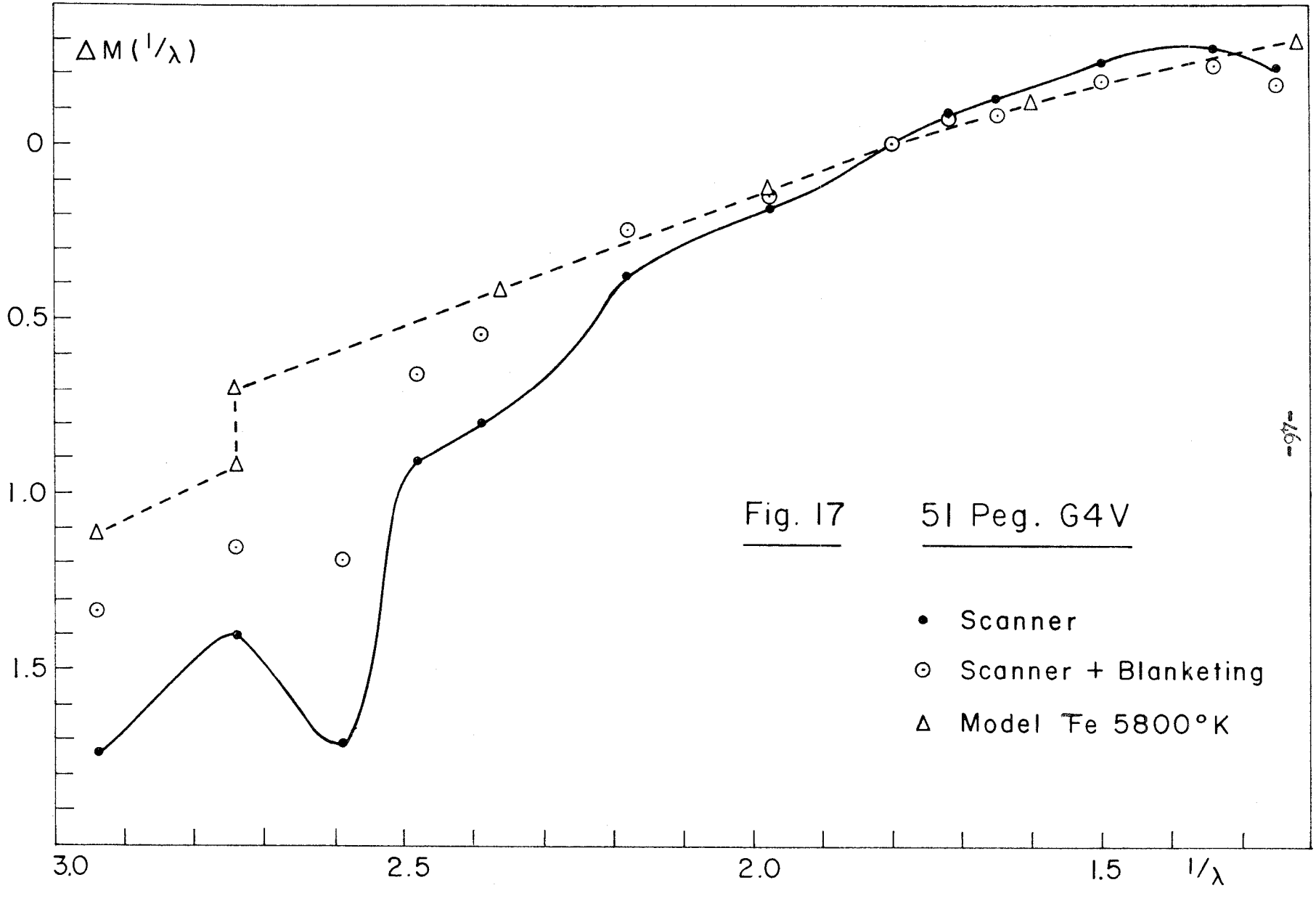
ΔM (1/λ)
0
0.5
1.0
1.5
3.0
2.5
2.0
1.5
1/λ
Fig. 17
51 Peg. G4V
Scanner
Scanner + Blanketing
Model Fe 5800°K

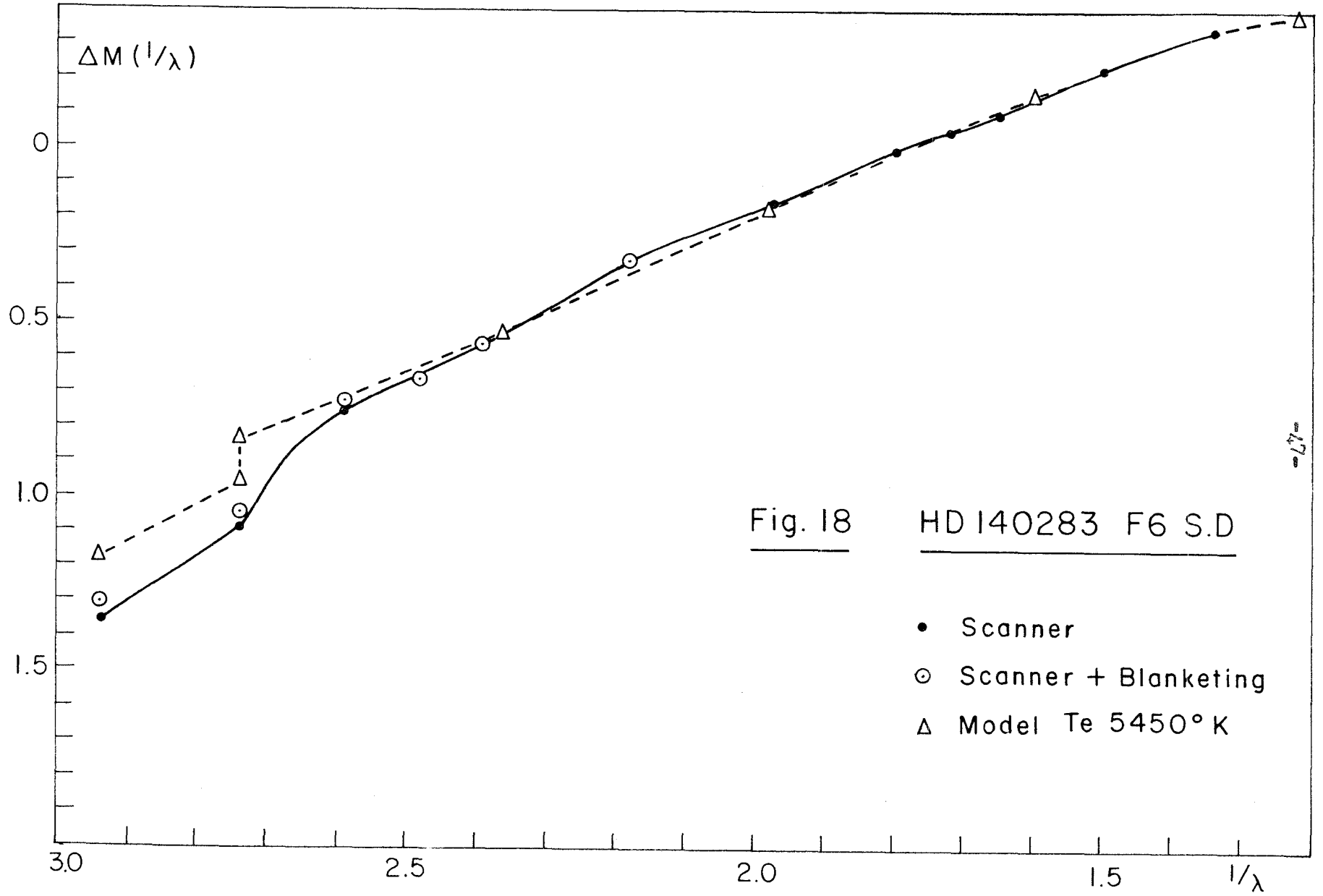
ΔM (1/λ)
0
0.5
1.0
1.5
3.0
2.5
2.0
1.5
1/λ
Fig. 18 HD 140283 F6 S.D
Scanner
Scanner + Blanketing
Model Te 5450° K

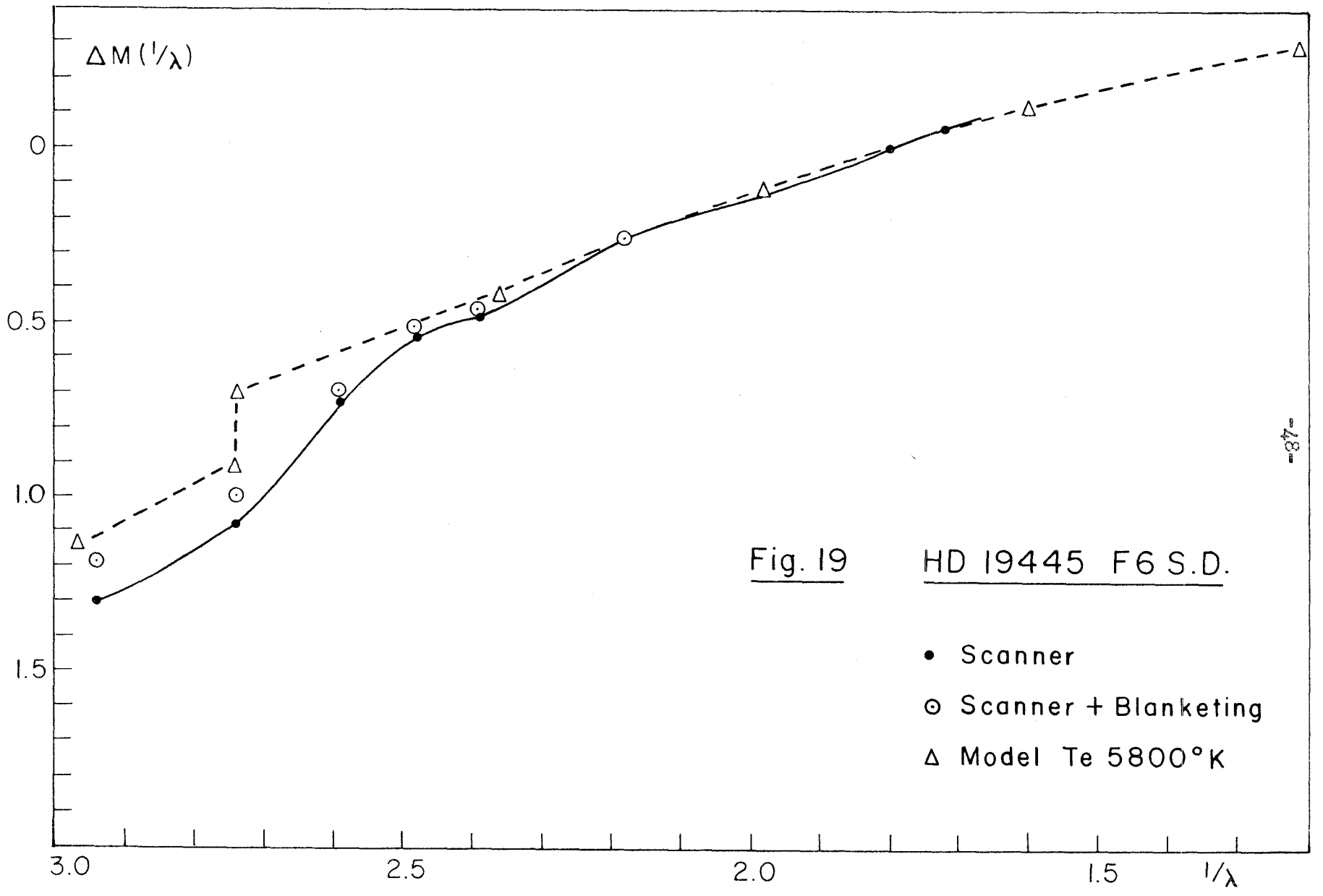
ΔM (1/λ)
0
0.5
1.0
1.5
3.0
2.5
2.0
1.5
1/λ
Fig. 19
HD 19445 F6 S.D.
• Scanner
⊙ Scanner + Blanketing
Δ Model Te 5800°K

observations are in error by $0^m.3$ in the far ultraviolet and should agree with the model implies a negative Balmer jump in later-type stars. On the other hand it is not unlikely that the α Lyrae magnitudes in the overall ultraviolet are fainter by $0^m.1$ than the true values. An argument for the existence of this difference is the consistent disparity of roughly this amount between the models and all the stars in this program. It could be maintained that the ultraviolet opacity values, for example, used in the computations are consistently small producing fluxes greater than the observed. It is difficult to understand, however, how such an error could prevail more or less constantly over a range of temperatures of 5000° k within which the dominant source of opacity shifts from H to H^- and moreover, apparently be independent of metals abundance particularly in the cooler stars. A $0^m.1$ error the absolute calibration results would seem at present to be the more attractive hypothesis.

It is not surprising that the A0 V model deviates from the observed distribution to the extent that it does. Certainly, the assumption of a grey body temperature distribution for such a star is of questionable validity with respect to the accuracies involved. In the region $\lambda<3647$ one sees a very short distance into the star because of the large opacity, ie., the observed flux emanates primarily from layers above $\tau = 0.1$. Therefore, any change in the temperature distribution or more specifically, the boundary temperature, will affect this ultraviolet region considerably. Furthermore, because of the extreme Balmer and Lyman absorption lines and the corresponding decrements it is quite likely that the actual boundary temperature lies significantly below the grey body value providing a lower observed ultraviolet flux.

A reasonable explanation (or rationalization) of the disagreement in the region $\lambda > 3647$ is not so forthcoming. Again, it seems unimaginable that the observations are the sole cause of the differences since this region (except the ambiguous region around λ 3700) is one in which more reliable results are available. Forcing agreement here also causes severe disagreement in the remainder of the program stars except β Ari. The point $\frac{1}{\lambda} = 2.59$ is understandably low because it lies half way between H_η and H_ϵ whose wings overlap. The receiver used in these measurements has a finite band pass and the resulting measurements are suppressed accordingly.

The points at greater wavelengths should not be affected by the adjoining hydrogen lines. It is interesting to note that β Ari shows the same disparities but to a smaller degree while in the next cooler star, σ Boo, they have become stationary remaining roughly the same for the rest of the stars. This would indicate that the variable part of the disparities is due to inaccuracies in the models. The models for α Lyr and β Ari were computed independently but using the same hydrogen opacity tables. The 10,700° k model by S. Saito (1956) includes electron scattering but the grey body temperature distribution was used and therefore does not imply flux constancy. In Osawa's 8900° k model electron scattering being negligible is not included but flux constancy is required. Neither of these refinements are capable of accounting for the excess in blue flux. There is the unlikely possibility the theoretical hydrogen opacities are under-evaluated. Still another possibility is that the actual temperature distribution is severely perturbed by the generally non-grey opacity or by convection which commences in these models around $\tau = 0.1$.

In the infrared regions of α Lyr past λ8206 there is a clear case implying the published flux distribution is inaccurate. The scatter of the observations in this region makes it difficult to derive a flux distribution with confidence. The opacity longward of the Paschen limit is less than it is on the blue side of the limit. The color temperature should therefore be greater on the red side. The respective slopes of the model around the Paschen limit agree at least qualitatively with this argument but observations do not. Indeed, the slope of the observed distribution implies a greater opacity past the limit while the strength of the flux in this region implies the contrary.

These problems have been discussed not with the purpose of attempting to ascertain the cause of the difficulties but rather to emphasize their existence. The fact the model does not accurately represent the true flux distribution of α Lyr is of secondary importance in this investigation. What is of concern, however, is how accurately the observed distribution agrees with the true distribution; any errors in these measurements are exhibited by all the stars in the program. It is the writer's opinion that the α Lyr monochromatic magnitudes are in error in the ultraviolet by roughly $0^m.1$ and that this quantity diminishes to about zero around $\frac{1}{\lambda} = 2.4$.

It is also felt that the infrared values are erroneous and should coincide closely with the model. The published values have been used, however, to construct Figures 11 through 19 and Table II. Because the questionable infrared results the curves have been terminated at $\lambda 8000$. In passing it should be remarked that there is also an observational difficulty in the infrared with atmospheric water vapor bands. It is also suspected for later types that additional continuous opacities are effective in this region. In the stars β Com, 51 Peg and other late types observed by Code localized depressions have been found which seem too large to be fully explained by either of the above two effects. There is also the Chalonge discontinuity near 5000A which is apparent in the figures by the systematically lower value at $\frac{1}{\lambda} = 1.98$ and discussed by Code (1959).

As mentioned above the observed monochromatic magnitudes are consistently below the theoretical curves in the ultraviolet for all the stars. For the later spectral types crowding of absorption lines in the ultraviolet and consequent suppression of the apparent continuum has caused the blanketing measurements to be lower than the true values. This effect is incipient in the far ultraviolet measures of the F6V stars and becomes pronounced in β Com. The star 51 Peg undoubtedly shows line crowding out to $\lambda 5000$. The cyanogen band at $\lambda 3900$ in this star is an extreme example of this effect.

The overall agreement between the models and the blanketing compensated distributions does leave room for improvement. On the other hand, the agreement is significantly better than the comparison with the scanner curves alone. It is encouraging that the effective temperatures of the models giving the best fit are comparable although slightly higher than the established temperature scale for main-sequence stars (Hynek 1951). The systematic difference stems from the fact that the absorption lines in these stars causes more flux to radiate in the continuum regions. To estimate the actual effective temperature of a star one must measure the total amount of line absorption throughout the spectral distribution and employ equation 1.

The total absorption may be adequately determined in the following manner. The circled points in Figures 11 through 19 define a blanketing compensated curve. However, in many of the regions between the measured wavelengths the line absorption is greater. It will be recalled that the wavelength points were selected primarily on their merit of being free or

nearly free of strong line absorption and yet giving a fair sample of the energy distribution. Therefore, if one were to transform every point on a scanner tracing to $a\Delta M(\frac{1}{\lambda})$ curve one would find many regions where the transformed curve falls below the smoothed monochromatic magnitude curve. The difference between this curve and the curve defined by the circled points is a measure of the absorption at any wavelength and the integral of this difference over the distribution is then the total blanketing in the observable region. A practical way of measuring this is to connect the measured points on the scanner recording such that the connecting line is commensurate with the $\Delta M(\frac{1}{\lambda})$ scanner curve. The percentage difference between this line and the tracing is an indication of the additional absorption which must be taken into account. The numerical integrations may be adequately accomplished with integration intervals from 0.05 to 0.1 μ^{-1}. To obtain the proper ordinate for each interval the scanner recording is divided into the same integration intervals. A measurement of the area in an interval between the connecting and scanner lines divided by the total area under the tracing yields the percentage by which the particular ordinate value should be decreased. This procedure is valid if the response function of the receiver does not radically change over the integration interval. (It might be objected that this procedure which is accurate to about 1% is too elaborate to follow simply to obtain flux corrections for the temperature estimates. However, these results are also used in the following chapter in the analysis of stellar colors.) This new ordinate subtracted from the corresponding ordinate on the blanketing curve yields the difference to be integrated. Table IX lists the results of these calculations as well as the model and corrected effective temperatures. In this table ΔF is formally defined by the relation

$$\Delta F(o) = \int_o^\infty \left| F_\nu^{(3)} - F_\nu^{(1)} \right| \, d\nu \quad , \tag{24}$$

where $F_\nu^{(3)}$ and $F_\nu^{(1)}$ are the blanketing compensated and corrected scanner fluxes, respectively. The quantity F is the total flux from the star and is defined by the relation

$$F = \sigma T_e^4/\pi \quad . \tag{25}$$

Table IX

EFFECTIVE TEMPERATURES

Star	Model T_e	$\Delta F/F$	T_e
α Lyr		0.05	
β Ari	9500	0.060	9350
σ Boo	6800	0.057	6700
π^3 Ori	6750	0.065	6650
110 Herc.	6550	0.089	6400
β Com.	6100	0.10	5950
51 Peg.	5800	0.12	5600
HD140283	5450	0.005	5450
HD19445	5800		5800

For the stars α Lyr and β Ari the chief contributors to the total blanketing are the hydrogen lines. Undoubtedly, the Lyman line contribution is not negligible in α Lyr and ΔF will be correspondingly greater. Between the spectral types A5 and F2 the transition occurs from the Balmer to the metallic lines as the primary contributors. Although line absorption becomes quite severe in the ultraviolet in the later types its effect on the blanketing is mitigated somewhat by the shifting of the spectral distribution to the red. In 51 Peg, for example, the actual blanketing coefficients in the ultraviolet certainly average at least 50%; but the total flux removed by the lines is only 12%. Similarly, the Lyman lines become stronger with later type but this is offset by the little energy in this region.

One of the more interesting results of this investigation is the corroboration of the significantly cooler temperatures ascribed to the sub-dwarfs (Code, 1957; Bahng, 1958). An F6V star has a nominal effective temperature of 6400 k and although HD140283 carries a middle F-type classification its effective temperature is a 1000°k cooler rendering it equivalent to a G6V star. These results are further discussed in the following chapter.

Evaluation of the method for determining effective temperatures.

The use of this method to determine the effective temperatures of other classes of stars affords an interesting possibility. In this analysis simultaneous use of the observed energy distributions, the blanketing measurements and the theoretical spectral distributions has been made in order to investigate stellar effective temperatures. The method is only as good or accurate as the least accurate of the above three factors. The group of stars under study is considered the 'safest' from the above standpoint

(and consequently that group which is best understood). The method at present is effective for late A through middle G type stars.

At the higher temperatures our theoretical knowledge at present seems insufficient to obtain good temperature estimates. Also, at the earlier types the energy distribution becomes less temperature sensitive and the increments of temperature change become increasingly large with earlier spectral type, the latter of course being an empirical effect. There is, of course, the further disadvantage that we can at present observe only the tails of the energy distributions of those stars.

At the cooler limit the observational difficulties in the visible region become very complex. The blanketing measurements become hopeless since strong overlapping of lines wipes out any trace of the real continuum. The scanner tracings become almost chaotic in some regions presenting an over-all jagged and uneven appearance making it increasingly difficult to accurately match the tracings and the blanketing coefficients. Perhaps a promising area of investigation of late types is an analysis such as this one working solely in the far red and infrared even past 10,000A. As implied above, the heavy blanketing for some late types may not be as damaging to the validity of the separation of continuous and discrete opacities as it would at first seem. For a star of 5000 k roughly only 20% of the continuous flux is emitted in the spectral regions less than 4000A so the total flux removed by the lines is probably only 15% or so. The disadvantages to this region are the possibility that the terrestrial absorption bands may be troublesome and the fact that the region requires receivers with surfaces such as the PbS surface and which are lower in sensitivity than the S4 or tri-alkali surfaces.

From the observational standpoint this method may be readily extended to A, F and G stars of other luminosity classes although, the wider dispersion in chemical composition and mass in the giants may cause some ambiguity in associating the spectral classification scheme with an effective temperature scale.

V. THE EFFECT OF BLANKETING ON STELLAR COLORS

1. Computations

Because of the importance of the role of stellar colors in astronomy knowledge of the blanketing effect on stellar colors is of obvious value when the colors are applied to astrophysical problems. At the present time the UBV system of Johnson and Morgan (1953) is a standard photometric system and is the one used in this investigation. This three-color system is accurately defined by a list of standard stars whose colors have been carefully measured in this system. On the other hand one should be able to define this system physically in terms of the response functions of the receiver with the three filter systems employed. With this information one may compute the B-V and U-B colors of standard stars whose energy distributions are known and expect to obtain agreement with the standard list. The effect of blanketing on stellar colors may be ascertained by integrating the absorption line-free fluxes as well as the observed distributions. The theoretical fluxes may also be integrated and their colors should, ideally, agree with the line-free (including the Balmer lines) colors.

The UBV photometric system is physically defined by the following specifications on the receiver. An RCA 1P21 surface and two aluminum surfaces are employed with the following filters: U = Corning 9863, B = Corning 5030 + 2 mm. Schott GG13 and V = Corning 3384. The sensitivity functions of the 1P21 with these filters without the aluminum reflection have been published by Johnson and Morgan (1951).

It turns out that the published data on the U system extends slightly farther on the ultraviolet side than the atmospheric cut-off. The observed U response extrapolated to zero air mass will therefore not coincide with the computed value. In order to insure compatibility between the computed and observed U response it is necessary to fold the atmospheric extinction relation into the sensitivity function, compute the response at two or more air mass values and extrapolate to zero air mass. The atmospheric extinction relation may be readily obtained from the standard Rayleigh extinction law or the curve in Table I with the ozone absorption included in the ultraviolet. (Concerning the latter effect confer, for example, Allen, 1955). Table X lists the response functions of the UBV system including two aluminum reflections for zero, one and two air masses as constructed by Code. In this

table S is the sensitivity function of the filters plus two aluminum reflections and P is the extinction term. The additional air mass values for the Band V filters have been listed for completeness. It may be directly verified from the sums at the bottom of this table that the direct and the extrapolated U response will differ by roughly $0^m.1$.

Although equation 3 was defined with the narrow band pass of the scanner in mind it applies as well to wide band photometry. With this equation one obtains the computed colors C_u and C_y, through the relations

$$(25) \qquad C_u = C(U) - C(B) = 2.5 \log \left[I(B)/I(U) \right] \quad ,$$
$$C_y = C(B) - C(V) = 2.5 \log \left[I(V)/I(B) \right] \quad .$$

The UBV system has zero points determined by six AOV stars whose mean U-B and B-V colors are defined to be zero. With this definition the above colors are related to the U-B and B-V colors through the relations

$$(26) \qquad U-B = C_u - 1.120$$
$$B-V = C_y + 1.040 \quad ,$$

given by Johnson and Morgan (1953).

The observed fluxes contained in Table II were corrected for the line absorption on the scanner tracings and the integrations were performed numerically as outlined in the previous chapter. Table XI lists the computed stellar magnitudes in the three filter systems relative to λ 5560, the computed and observed U-B and B-V colors and the differences between them. The U-B and B-V differences are nearly constant having RMS fluctuations of $0^m.04$ and $0^m.02$, respectively which are commensurate with the accuracies of the scanner observations.

There appears to be a slight systematic effect with spectral type which tends to give smaller computed ultraviolet colors for the stars with strong hydrogen lines. The possibility of an over-estimation in these stars for the effect of hydrogen lines in the ultraviolet numerical integrations of the scanner tracings was considered. It turns out that the probable error in these estimates is at most $0^m.01$ or $0^m.02$. An alternate explanation for

Table X

RESPONSE FUNCTIONS OF THE UBV SYSTEM

$1/\lambda$	$S(U)$	$S(U)p^{(1)}$	$S(U)p^{(2)}$	$S(B)$	$S(B)p^{(1)}$	$S(B)p^{(2)}$	$S(V)$	$S(V)p^{(1)}$	$S(V)p^{(2)}$
3.40	0.000	0.000	0.000						
3.30	0.819	0.066	0.025						
3.20	1.755	0.346	0.091						
3.10	2.598	0.777	0.229						
3.00	3.360	1.300	0.497						
2.90	3.925	1.813	0.852						
2.80	4.071	2.178	1.181	0.000	0.000	0.000			
2.70	3.916	2.330	1.382	0.126	0.075	0.044			
2.60	2.201	1.426	0.918	0.987	0.640	0.412			
2.50	0.282	0.197	0.136	3.620	2.523	1.745			
2.40	0.000	0.000	0.000	3.971	2.915	2.152			
2.30				3.909	3.006	2.306			
2.20				3.358	2.683	2.139			
2.10				2.457	2.015	1.658	0.000	0.000	0.000
2.05				(1.99)	(1.64)	(1.40)	0.135	0.112	0.093
2.00				1.529	1.286	1.079	1.181	0.993	0.834
1.95				(1.04)	(0.91)	(0.76)	2.478	2.104	1.779
1.90				0.589	0.505	0.431	3.251	2.789	2.380
1.85				(0.23)	(0.20)	(0.17)	3.246	2.808	2.425
1.80				0.000	0.000	0.000	2.854	2.486	2.166
1.75							2.269	1.990	1.745
1.70							1.719	1.518	1.341
1.65							1.044	0.930	0.828
1.60							0.526	0.473	0.426
1.55							0.202	0.183	0.167
1.50							0.108	0.099	0.090
1.45							0.053	0.049	0.045
1.40							0.023	0.021	0.020
1.35							0.000	0.000	0.000
Σ :	22.927	10.433	5.311	20.546	15.648	11.966	19.089	16.555	14.339

this effect is contingent on the possibility that the 15Å band pass of the scanner is somewhat larger than the band pass of the receiver used in the absolute calibration of αLyr in the ultraviolet. The point λ3860 situated midway between H_η and H_ϵ is affected by the wings of these lines when they are strong and the scanner, possessing the larger band pass, would register a smaller deflection than the absolute receiver. For stars with weaker hydrogen lines the overlapping wings would diminish the deflections less with the result that when these stars are compared with αLyr a measured flux at λ3860 larger than the actual flux would be forthcoming. The spectral region contributing most to the U response is around λ3860 and the flux value at this point is crucial in determining the distribution curve between λ3650 and λ4040. If this is, in fact, the source of the systematic trend the mean difference between the observed and the computed U-B colors is probably nearer $-0^m.12$ instead of the $-0^m.17$ obtained from Table XI. The mean of the differences in the B-V colors is $+0^m.13$. The results for two additional stars, 10 Lacertae and 16 Cygni A included in the list have been obtained from similar computations by Code (1959). A discussion of these results follows in the next section.

Table XI

COMPUTED AND OBSERVED STELLAR COLORS

Star	C(U)	C(B)	C(V)	$(U-B)_c$	$(B-V)_c$	$(U-B)_o$	$(B-V)_o$	$\Delta(U-B)$	$\Delta(B-V)$
α Lyr	+0.14	-0.85	+0.05	-0.13	+0.14	-0.01	0.00	-0.12	+0.14
β Ari	0.38	-0.70	0.07	-0.04	0.27	+0.10	+0.14	-0.14	0.13
σ Boo	0.46	-0.45	0.08	-0.21	0.51	-0.09	0.37	-0.12	0.14
π^3 Ori	0.55	-0.39	0.09	-0.18	0.56	+0.00	0.46	-0.18	0.10
110 Herc.	0.57	-0.35	0.08	-0.20	0.61	+0.00	0.46	-0.20	0.13
β Com	0.75	-0.22	0.11	-0.15	0.71	0.05	0.56	-0.20	0.15
51 Peg.	0.97	-0.17	0.09	+0.02	0.78	+0.20	0.68	-0.18	0.10
HD140283	0.37	-0.33	0.08	-0.42	0.63	-0.28	0.51	-0.14	0.12
HD19445	0.36	-0.39	0.07	-0.37	0.58	-0.24	0.46	-0.13	0.12
10 Lac				-1.26	-0.08	-1.04	-0.20	-0.22	0.12
16 Cyg A				-0.05	+0.78	+0.19	+0.64	-0.24	0.14

The line-free flux distributions were obtained from the curves defined by the circle points in Figures 11 through 19. The Balmer lines are for the present also excluded in these distributions so near the Balmer limit where the confluence of the hydrogen lines depressed the observed continuum the line-free distribution was continued along an extrapolated continuum to

the Balmer limit whence it was diminished to the λ3650 value. Similarly, for the spectral regions of those stars where it is obvious overlapping absorption lines are suppressing the continuum the curve was drawn at a more likely level determined primarily by the slopes of the model curves and the flux levels in the neighboring regions.

In Tables XII and XIII are exhibited the results of the integrations of the line-free and the theoretical fluxes. Columns 5 and 6 of Table XII are the differences in the computed colors of the stellar and the line-free flux distributions, while the last two columns are the line-free colors obtained by adding these differences to the observed colors. The parenthesized entries in Table XIII were obtained by interpolation in Table VII.

Table XII

COLORS OF THE LINE-FREE DISTRIBUTIONS

Star	C(U)	C(B)	C(V)	$\delta(U-B)_{H+K}$	$\delta(B-V)_{H+K}$	$(U-B)_{H+K}$	$(B-V)_{H+K}$
α Lyr	−0.24	−0.34	0.05	−0.29	−0.09	−0.30	−0.09
β Ari	−0.07	−0.85	0.07	−0.30	−0.15	−0.20	−0.01
σ Boo	+0.12	−0.57	0.07	−0.22	−0.11	−0.31	+0.26
π^3 Ori	0.06	−0.59	0.05	−0.29	−0.16	−0.29	0.30
110 Herc.	0.10	−0.53	0.05	−0.29	−0.15	−0.29	+0.31
β Com.	0.14	−0.48	0.04	−0.35	−0.19	−0.30	0.37
51 Peg.	0.65	−0.47	0.03	−0.49	−0.24	−0.29	0.44
HD140283	0.40	−0.34	0.08	−0.03	−0.01	−0.31	0.50
HD19445	0.41	−0.41	0.07	−0.07	−0.02	−0.31	0.44

Table XIII

COLORS OF STELLAR MODELS

T_e	C(U)	C(B)	C(V)	U-B	B-V
(4900)	+0.44	−0.19	+0.08	−0.48	+0.77
(5200)	0.33	−0.26	0.08	−0.53	0.70
5500	0.25	−0.34	0.07	−0.53	0.63
5800	0.17	−0.42	0.07	−0.53	0.55
6100	0.12	−0.47	0.07	−0.53	0.50
6400	0.06	−0.53	0.06	−0.53	0.45
(6700)	0.02	−0.58	0.06	−0.52	0.40
7000	0.00	−0.63	0.06	−0.49	0.35
7560	−0.02	−0.70	0.06	−0.44	0.28
(8200)	−0.09	−0.81	0.05	−0.40	0.18
8900	−0.19	−0.91	0.03	−0.40	0.10
(9500)	−0.28	−0.95	0.03	−0.45	0.06
10,700	−0.48	−1.00	0.03	−0.60	0.01

ii. Discussion of Results

Figure 20 is a graphical representation on the U-B, B-V plane of the results of these computations. The lower solid curve is the locus of points defining the main-sequence as taken from Johnson and Morgan (1953). The upper solid curve defines the computed colors of the models as listed in Table XIII. Also plotted on this figure are the observed and line-free colors of the program stars.

The model curve shows some interesting features which are primarily due to the Balmer discontinuity. Indeed, the shape of this curve might be fairly well inferred by simply studying the motion with effective temperature of the $\Delta M(\frac{1}{\lambda})$ points in Figure 10 at $\lambda 3647^{-}$, $\lambda 3647^{+}$ and $\lambda 4350$. The dip occurs in the region of maximum discontinuity. Towards cooler temperatures the curve emerges from the dip and assumes a horizontal slope which may be interpreted as being due to the rapid abatement of the discontinuity in conjunction with an increasing slope of the flux distribution. Although models only as cool as 5500° K have been computed it would seem fairly safe to extrapolate a ways to cooler temperatures on the basis of the rate of change of the slope of the distributions as well as the vanishing rate of the discontinuity. The dashed curve extending to 4900° K shows the turn-over region where the discontinuity becomes insignificant. Although the further extension of this curve is uncertain at this time without computing the corresponding models it would seem that because of the predominance of the smooth H^{-} opacity the curve should begin to assume a slope similar to a black body. It is pointed out that the line-free colors as discussed here have been obtained by considering only the direct effect of the hydrogen and the metallic lines. The small secondary effect due to the increased color temperature of the continuum with increasing line strength has up to now been ignored. This factor as well as the effect of the metallic lines alone is discussed presently in a following section.

The line-free colors as shown in this figure being derived from accurate measures are themselves quite reliable. The observed stellar colors possess probable errors of less than $0^{m}.01$. Moreover, the blanketing coefficients are accurate to 1% while the determinations of the line-free distribution and the numerical integrations are good to 1 or 2%. Since the errors in the sensitivity functions or in the absolute calibration (or scanner tracings)

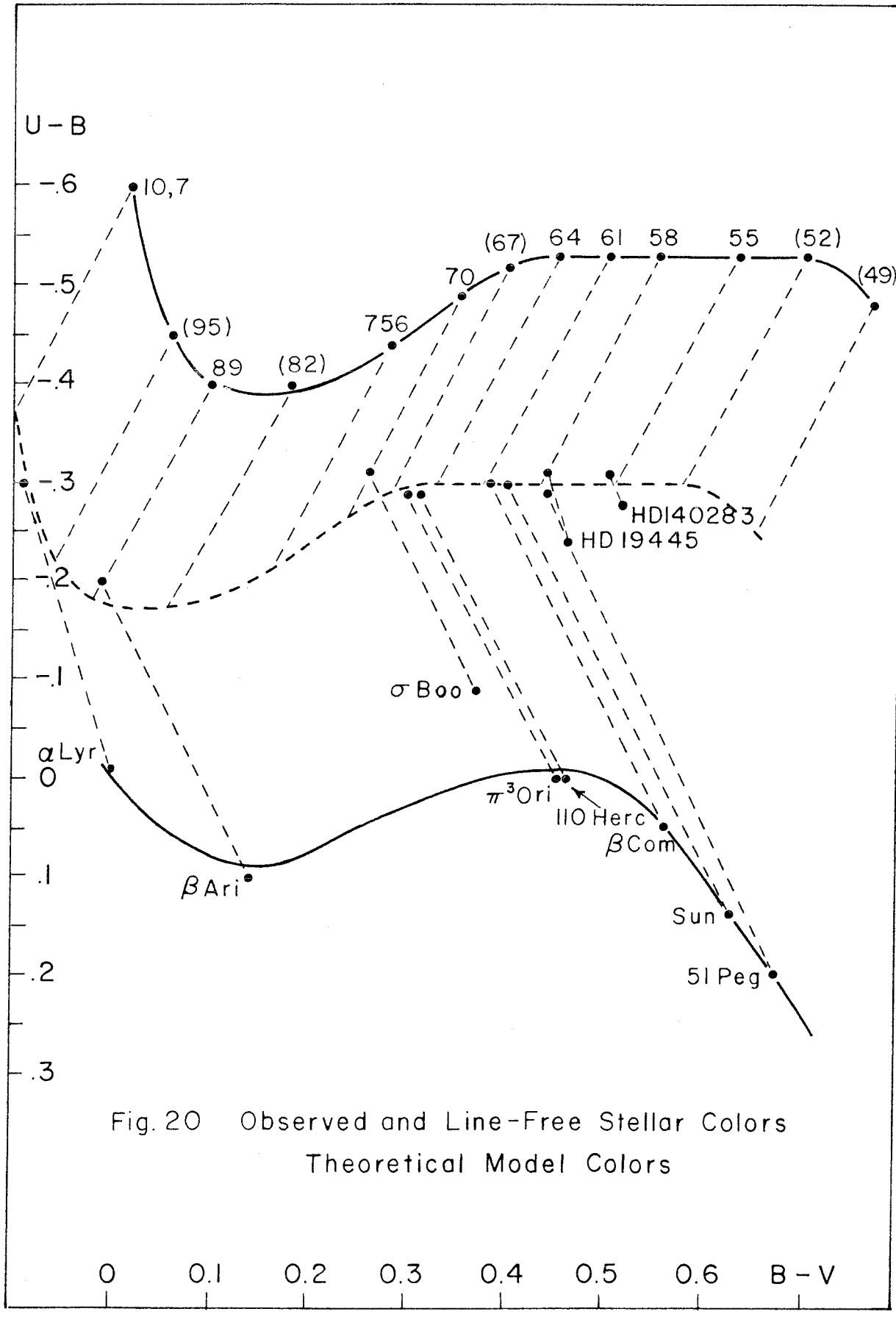

Fig. 20 Observed and Line-Free Stellar Colors
Theoretical Model Colors

nearly cancel* in the differences between the computed stellar and the computed line-free colors, these differences when applied to the observed colors yield semi-empirical line-free colors which have uncertainties of probably around $0^m.02$.

Thus, the main-sequence curve, the coordinates of the observed and the line-free colors are accurately placed on this U-B, B-V plane. Since the model curve should coincide with the line-free curve it follows that the computations leading to the model curve are in error. In order to bring them into the best agreement the model curve must be translated $-0.12 \pm .01$ in the B-V direction and $+0.23 \pm .01$ in the U-B direction. The dashed curve is this translated model curve. With this translation the agreement is excellent for $B-V > 0^m.25$ with some disparity remaining around α Lyr and β Ari. Not only is this translated model curve in coincidence with the line-free colors of the middle-type stars but there is also fine and consistent agreement, generally within 50 k, between the temperatures on this curve and the values found in Chapter 4 or ascribed from the established temperature scale for these stars. It should be recognized that this rather hybrid method of temperature determination which is an extension of the work by Bonsack et al (1957) is to the first order independent of the observed spectral distribution and therefore in a sense independent of the method employed in Chapter 4. The basis for the translation will be discussed shortly. But aside from these ensuing arguments there is validity in the single assertion that the model curve must be translated for the sake of agreement. The fact that this results in uniform temperature agreement is both a useful dividend and indicative of the general quality of the models and the fact that the error source leading to the translation is temperature independent. Observationally, the calibration of this method requires the determination of the stellar colors and the line-free colors through blanketing measurements not only in the B-V but the U-B as well. The latter is of course necessitated by the existence of stars of varying metals abundances and as represented in in Figure 20 by σ Boo, HD140283 and HD19445. Concerning the latter two stars

* Although one may easily generate the error coefficients for the above differences in a formal expression in terms of the possible error sources, a more practical way of verifying the reliability of these differences is to apply the blanketing coefficients to the model fluxes, compute the corresponding colors and obtain the differences between these and the model colors. The difference in the results using these two approaches amounted to only $0^m.01$ to $0^m.02$ in the cases tried.

it is seen that again temperature values corresponding to G-stars result with the hotter star HD19445 being very similar to the actual effective temperature of the sun. (Anticipating the results of a following section one finds for the line-free position of the sun U-B = $-0^{m}.30$ and B-V = 0.40 corresponding to a continuous flux temperature of 5950° k.) Finally, there would seem to be at present a rather serious inability of the spectral classification schemes to quantitatively isolate main-sequence stars of different metals abundances. Even the mildly deficient star σ Boo, seems to have a temperature some 200° K cooler than the 7000° K attributed to a normal F2V star and, of course, the two sub-dwarfs are extreme and long recognized manifestations of this effect.

iii. The Systematic Differences Between Theory and Observation

The differences between the computed stellar colors in Table XII and the observed colors should average to zero. The fact that they significantly do not indicates the published sensitivity functions or the monochromatic fluxes used in the integrations are in error. Similarly, the error causing the required translation in Figure 20 can arise only from the sensitivity functions or the theoretical fluxes. There are, then, three candidates as error sources: the sensitivity functions, the absolute calibration of α Lyr and the models. There is insufficient information present to uniquely isolate the causes of the discrepancies, although as will be seen, there is a strong case for suggesting that the main error source lies in the sensitivity functions. The sensitivity functions and to a lesser degree the absolute calibration are readily amenable to further refinements given enough careful and diligent measurements.

For the present, perhaps the best course of action is to consider the implications which result from attributing errors to these quantities subject to the constraints that the errors must sum to give:

1. the differences between the observed and the computed stellar colors, $\Delta(U-V) = -0^{m}.05$, $\Delta(B-V) = +0^{m}.13$
2. the required translation in Figure 20, $\Delta(U-V) = +0^{m}.11$, $\Delta(B-V) = -0^{m}.12$.

Consider what follows if it is assumed the absolute calibration is the source of the differences in condition 1. This would require the flux distribution of α Lyr to be more than $0^{m}.1$ brighter in the blue regions; this is

significantly greater than the probable errors of the absolute measurements in this particular region. (Confer Figure 4, Code, (1959)). Still another consideration is that such an error would imply a Balmer discontinuity much greater than indicated from observations particularly for very early type stars. Furthermore, from this assumption it also follows that the translation values in condition 2 are due solely to errors in the models. To eradicate this error a rotation is required of the theoretical flux curves about the point $\frac{1}{\lambda} = 1.8$ such that the values at $\frac{1}{\lambda} = 2.3$ (the effective wave numbers of the V and B filter systems, respectively) are about $0^{m}.1$ stronger and such that the ultraviolet regions are $0^{m}.1$ weaker. Such a configuration leads to a Balmer discontinuity for the 5500°K model in excess of $0^{m}.3$ which is unacceptable. It is also felt that the precision of our knowledge of the continuous opacities is better than 10%. The assumption that the sensitivity[5] functions are free from errors leads at this time to rather untenable conclusions.

Code (1959) in discussing the differences between the computed and observed stellar colors has pointed out that a similar discrepancy exists in the six-color photometry of Stebbins and Whitford (1945). He suggests that the U and the V band passes of both photometric systems may be overestimated relative to the B and that this may stem from the fact that the sensitivity functions of both systems were calibrated with the same monochromator and thermocouple at Washburn Observatory. He has further pointed out that Tifft's (1958) and Bahng's (1958) multicolor data do not show this discrepancy and that they were both calibrated with different monochromators and thermocouples. Notice that the B-V differences are essentially identical; that is, attributing a B-V error of $+0^{m}.12$ to the sensitivity functions eliminates the B-V discrepancies in both Table XII and Figure 20. Attributing a U-V error of $-0^{m}.11$ to the sensitivity functions implies a $+0^{m}.06$ U-V error in the ultraviolet absolute calibration of α Lyr, which is nearly the mean of the difference noted in Figures 11 through 19. (The argument can as easily be altered so that this difference is due to model errors by allowing the U-V error in the sensitivity functions to be $-0^{m}.05$.)

It is provisionally asserted, subject to future revisions of the sensitivity functions of the α Lyr calibration, (and it should be noted that the accurate determination of any one of these quantities clears up the whole

problem), that the sensitivity functions are the principal error source and that the additional discrepancy noted around α Lyr and β Ari in Figure 20 is due to defects in the corresponding models. It is recalled from Chapter 4 that these models gave the poorest agreement with the observed flux distributions of these two stars.

There remains the question of why the translation employed in Figure 20 produces such uniformly good results. Suppose for the moment there exists an arbitrary error $\delta S_\lambda(R)$ in one of the sensitivity functions R. This quantity will manifest itself in the R response through the differential relation

$$(27) \qquad \delta R = -1.086 \int_{\lambda_1}^{\lambda_2} \delta S_\lambda F_\lambda d\lambda \Big/ \int_{\lambda_1}^{\lambda_2} S_\lambda F_\lambda d\lambda$$

$$= -1.086 \frac{\overline{\delta S}}{\overline{S}} \quad ,$$

where λ_1 and λ_2 are the limits of the R band pass and $\overline{S}$ and $\overline{\delta S}$ are the flux weighted means given by

$$(28) \qquad \overline{S} = \int_{\lambda_1}^{\lambda_2} S_\lambda F_\lambda d\lambda \Big/ \int_{\lambda_1}^{\lambda_2} F_\lambda d\lambda$$

and

$$(29) \qquad \overline{\delta S} = \int_{\lambda_1}^{\lambda_2} \delta S_\lambda F_\lambda d\lambda \Big/ \int_{\lambda_1}^{\lambda_2} F_\lambda d\lambda \quad .$$

It may be directly verified that within the temperature range under consideration $\overline{S}(U)$ is constant to within 1% while $\overline{S}(B)$ and $\overline{S}(V)$ are constant to about 5%. Furthermore, although δS_λ has been assumed arbitrary in the actual case it is undoubtedly no more radically distributed than S_λ and probably possesses a flatter distribution; in either case it also is constant to within a few percent. The conclusion to be drawn from these considerations is that over this temperature range $\Delta(U-V)$ and $\Delta(B-V)$ are constant to better than 10% (and probably much less since the variable components in the mean values tend to cancel.) This explains the general effectiveness of the translation since $\Delta(U-B)$ and $\Delta(B-V)$ change only $0^m.01$ or $0^m.02$ over the whole temperature range.

iv. The Effect of Metallic Line Blanketing on Stellar Colors

Historically, the value of the main-sequence in the color-magnitude diagram as an analytical tool was derived fundamentally from the premise that the chemical composition was essentially invariant among the stars. In recent years it has become abundantly clear that there exist significant differences in chemical composition among main-sequence stars and that, for example, the main-sequence stars in the solar neighborhood form a more heterogeneous group than do the corresponding stars in a galactic cluster. The presence of sub-dwarfs below the main-sequence in a color-visual magnitude diagram is linked closely with the corresponding metallic deficiencies and ultraviolet excesses in this type of stars. It seems likely that groups or perhaps even systems of main-sequence stars exist whose metals abundances range from insignificant proportions to solar or slightly stronger concentrations.

The Johnson-Morgan UBV main-sequence (1953) is defined from the stars in the solar neighborhood. Of some importance, then, is the knowledge of the manner in which this main-sequence curve is altered as the metals abundance varies. Each group of homogeneous composition defines a main-sequence relation which is displaced from the relation for another group of different composition. Thus, one might expect a continuum of main-sequence relations whose boundaries correspond to the extremes in metals abundances which occur. To indeed establish a family of main-sequence curves corresponding to different chemical composition is naturely a formidable (and perhaps unrealistic) observational program and one for which only small progress has been made with the recent studies of galactic clusters.

What can be estimated, however, and what is partially done in this investigation is the extremes of this main-sequence continuum on the assumption that the blanketing effect of metallic absorption lines alone is responsible for the continuum and that the Johnson-Morgan main-sequence represents those stars with the highest metals concentration to be formed up to the present. The first problem at hand is the one of determining the U-B and B-V main-sequence for stars with metals abundances so low that the resulting absorption lines produce an insignificant effect on the colors.

Imagine one has available an ensemble of main-sequence stars of constant mass but of diverse metals abundances and consider the line defined by the

U-B and B-V colors of these stars. As stars of smaller abundances are observed the U-B and the B-V colors become stronger moving away from the main-sequence on a more or less diagonal line. The color temperature of the continuous flux diminishes producing a small secondary effect on the colors. Ultimately, this blanketing line terminates where the metals abundances has diminished to a point where it no longer affects the colors which is about a factor of 25 or so down from the solar abundances. This, of course, may be only part of the story. The helium abundance almost surely is correlated with the metals abundance and will produce an additional effect on the blanketing line by changing the effective temperature of stars. Still other ominous features are the complicating possibilities of a transfer in the stellar interiors from the bound-free metals opacity to free-free hydrogen and helium opacity, the existence of a convective envelope whose depth varies with abundance and in the earlier types the ultimate transfer from the carbon to the proton cycle. All that can be reproduced here is strictly the blanketing effect. Whereas the blanketing lines which were imagined above are lines of constant mass but not necessarily effective temperature, the lines to be generated presently are lines of constant temperature but not necessarily constant mass. These lines will coincide only if the effects of the above complications either are negligible or cancel. As will be seen there is some evidence to indicate that at least for mild departures from normal abundances the blanketing lines to be constructed do coincide closely with the 'empirical lines'.

In order to compute the effect of metallic lines on the colors the same procedure was followed as indicated in the first section with the exception that the effect of the hydrogen lines was removed. (The slight effect of varying the hydrogen line strength with metals abundance in cooler stars where the metals are the principal suppliers of electrons to the continuous opacity has been ignored and is considered to be negligible.) The change in the color temperature of the continuous flux due to metallic line absorption was found to vary from essentially zero for αLyr to 200° K for 51 Peg. To ascertain the resulting change in the colors due to this effect one need only consult the theoretical UBV relation as shown in Figure 20; it turns out the corrections range from $0^m.00$ to $0^m.04$ in B-V and zero everywhere for U-B.

Table XIV lists the small differences in B-V due to the temperature effect, the color differentials due to the total effect of the metallic lines and finally, the blanketing compensated colors which are obtained by applying the differentials to the observed colors.

Figure 21 shows the results of these calculations. The diagonal lines connecting the observed and the blanketing compensated colors are the blanketing lines and as pointed out above, are lines of constant effective temperature. One might also consider these lines as being generated by the parameter, log A. The curve drawn through the blanketing compensated points defines the upper limit of the main-sequence corresponding to metals-free stars. For temperatures cooler than about 6000°k this curve is identical with the line-free curve in Figure 20 since the hydrogen lines make a negligible contribution for cooler temperatures. The corresponding effective temperatures are indicated and the curve has been extrapolated to the cooler temperatures. The term "metals-free" is used figuratively since as pointed out above for stars with metals abundances of roughly five percent or less of the solar abundance the metallic lines have little effect on the colors. An interesting conclusion follows from the horisontal slope of this curve out to about 5000°k. The observed main-sequence turns down around 6200°k; this indicates that in this temperature range the drop in U-B is due solely to line absorption. The slope of the blanketing lines is not too unlike the slope of the observed main-sequence curve below 6000°k which is expected from the above consideration. They are not quite parallel and there is reason why they should not be; the main-sequence curve is produced by changing the temperature keeping the metals abundance constant while the blanketing lines represent constant temperature with varying abundance. On this basis one would expect the blanketing lines to be more steeply inclined which is the case. These lines have been depicted as straight for lack of further evidence. Their actual form aside from the additional factors which may affect them may depart somewhat from a straight line, although, the logrithmic nature of the color indices tends to remove the curvature. The departures from straight lines might be inferred from the different slopes of the sub-dwarf lines although the effect may not be significant. However, σ Boo which is apparently a mild sub-dwarf shows about the same slope as the remainder of the stars.

The colors of the sun which are included in this figure were derived in

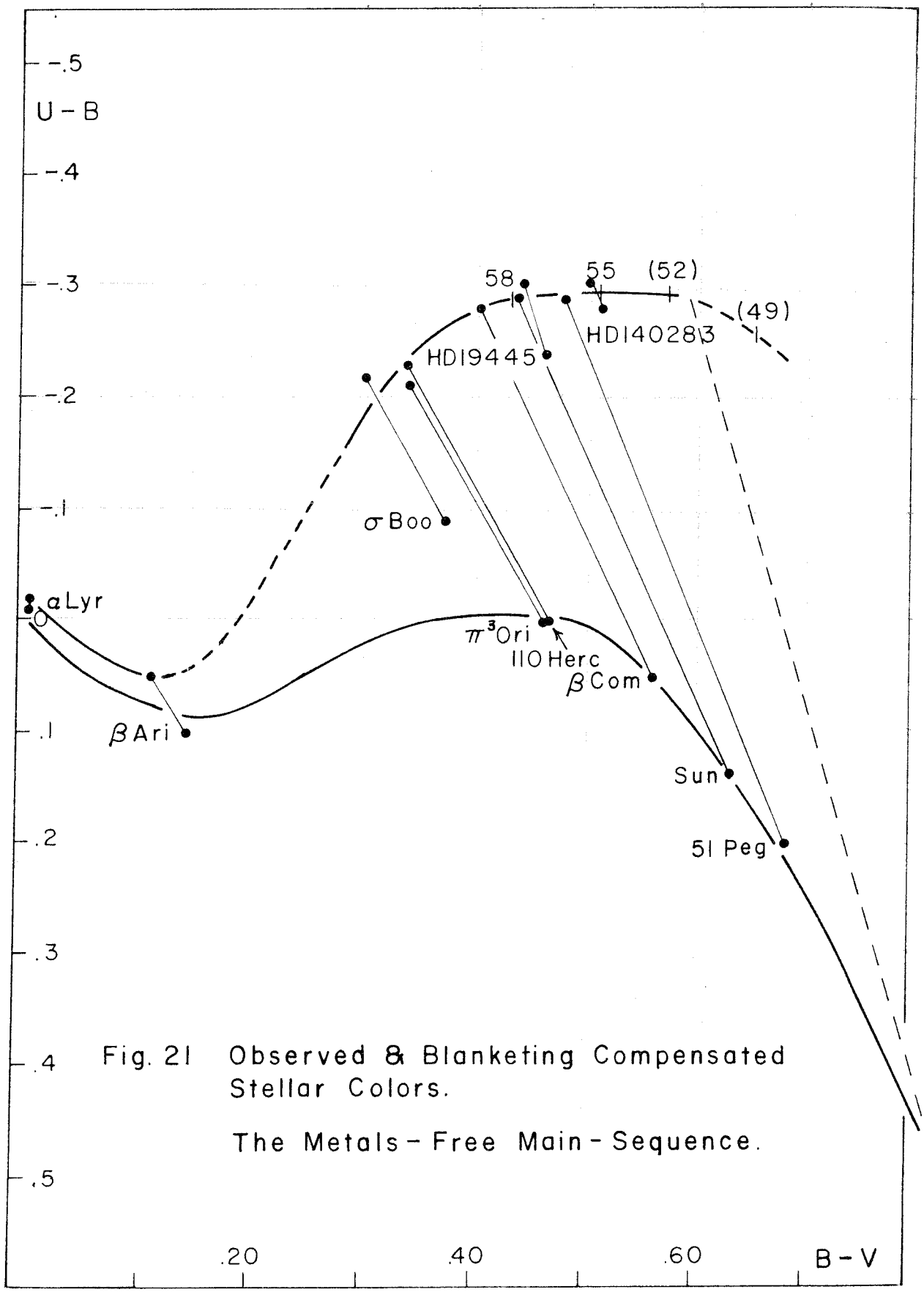

Fig. 21 Observed & Blanketing Compensated Stellar Colors.

The Metals - Free Main - Sequence.

Table XIV

BLANKETING COMPENSATED COLORS

Star	$\delta(B-V)_T$	$\delta(U-B)_M$	$\delta(B-V)_M$	$(U-B)_M$	$(B-V)_M$
α Lyr.	0.00	-0.01	0.00	-0.02	0.00
β Ari.	0.00	-0.05	-0.03	+0.05	0.11
σ Boo.	+0.01	-0.13	-0.07	-0.22	0.30
π^3 Ori.	0.02	-0.21	-0.12	-0.21	0.34
110 Herc.	0.02	-0.23	-0.13	-0.23	0.33
β Com.	0.03	-0.33	-0.16	-0.28	0.40
Sun	0.04	-0.43	-0.19	-0.29	0.44
51 Peg.	0.04	-0.49	-0.20	-0.29	0.48
HD140283	0.00	-0.03	-0.01	-0.31	0.50
HD19445	0.00	-0.06	-0.02	-0.30	0.44

a similar manner. The blanketing coefficients were obtained from the Utrecht atlas and applied to the observed flux distribution of 16 Cygni A, a G2V star. The remainder of the analysis follows in an identical fashion. Stebbins and Kron (1957) obtain from their six-color photometry of the sun a B-V color of $0^m.63$. They consider their ultraviolet determination to be somewhat questionable; upon transferring their results to the UBV system one derives a U-B of $0^m.07$ which places the sun slightly off the main-sequence. Although there seems to be some evidence to indicate the sun does have slightly weaker absorption lines it does not yet seem conclusive. Therefore, for the present the standard U-B color of $0^m.14$ is used; it will be seen that this value also leads to consistent results. The differential color corrections due to metallic lines was found to be $\delta(U-B) = -0^m.36$ and $\delta(B-V) = -0^m.21$ the latter value being $0^m.04$ larger than found by Schwarzschild, Searle and Howard (1955). The color temperature effect of the continuous flux removes $0^m.04$ from the B-V value. It will be recalled that the Utrecht atlas presents the spectrum of the center of the solar disk which is equivalent to a star about 200° K hotter. The blanketing coefficients derived from the atlas are close to those from a G0V star. In order to allow for this half the differences between the differential color corrections for β Com and 51 Peg were added to the solar values. This brings the final values of the color corrections to $\delta(U-B)_M = -0^m.43$ and $\delta(B-V)_M = -0^m.19$ yielding blanketing compensated colors for the sun of $(U-B)_M = -0^m.29$ and $(B-V)_M = 0^m.44$. This places the sun at a position which is compatible with the other stars in regard to effective temperature and also on the metals-free main-sequence.

There is an important conclusion which stems from a diagram such as Figure 21 which concerns the established empirical relationship between B-V and effective temperature. In applying the observed B-V colors to derive effective temperatures one must be quite sure of the kind of stars under study. Figure 21 shows the B-V can vary as much as $0^m.2$ for the same effective temperature or alternately, for a given B-V the temperature may range over a 1000^o K. The U-B, then, could supply the necessary third dimension to the empirical color-temperature relationship. By observing both the U-B and B-V colors one is able to place the star on a blanketing line. With the knowledge that the star is a main-sequence type one associates the effective temperature of this line with the star. This presumes, of course, that the blanketing lines have been properly calibrated by a method such as that employed in Chapter 4 or by infrared or other means.

By translating the star along its respective blanketing line to its intersection with the Johnson-Morgan main-sequence one may also determine the corrections in U-B and B-V necessary to place the star on this relation. The intersection becomes more difficult to determine for the cooler types because of the similarity in slopes of the blanketing and main-sequence lines. Table XV lists the required translations in B-V as a function of U-B and B-V. The parenthesized entries in this table have been derived from the extrapolation of the models. The fainter B-V entries are more uncertain because of this extrapolation and the nearly identical slopes of the UBV blanketing and main-sequence lines. The negative entries are included to suggest the possibility of overly abundant main-sequence stars.

Line blanketing may also affect the distance moduli and age estimates of clusters. Globular clusters have enhanced B-V colors by virtue of their metals deficiencies; this may affect reddening estimates, luminosity measurements of the break-off point and therefore age estimates. Certainly, fitting globular cluster main-sequences to the normal main-sequence is a dubious procedure; because of differential blanketing the two lines may be separated in absolute magnitude by as much as $1^m.0$. Furthermore, in comparing the ages of different globular clusters and to a lesser extent galactic clusters it is clear that one should consider the differences in metals abundances which occur among them.

Figure 21 is not so amenable to observational verification. One may

Table XV

B-V BLANKETING TRANSLATIONS

B-V \ U-B	-0.30	-0.25	-0.20	-0.15	-0.10	-0.05	0.00	0.05	0.10	0.20
0.20							0.04	0.01	-0.01	
0.25					0.06	0.04	0.02	0.00	-0.02	
0.30			0.10	0.08	0.05	0.03	0.01	-0.02	-0.04	
0.35		0.14	0.12	0.08	0.05	0.03	0.00	-0.02	-0.04	
0.40		0.14	0.11	0.08	0.06	0.03	0.00	-0.03	-0.05	
0.45	0.19	0.16	0.13	0.09	0.06	0.03	0.00	-0.03	-0.05	
0.50	0.22	0.20	0.16	0.13	0.09	0.04	0.00	-0.02	-0.05	
0.55	(0.22)	(0.19)	(0.19)	0.16	0.12	0.09	0.04	-0.01	-0.04	
0.60		(0.21)	(0.20)	(0.19)	(0.15)	0.12	0.09	+0.05	0.00	
0.65			(0.20)	(0.20)	(0.18)	(0.14)	(0.11)	0.08	0.06	-0.02
0.70							(0.17)	(0.14)	(0.11)	+0.05

check the colors in the catalog of the high velocity stars (Roman 1955). It is found that of the 80 or so stars with negative U-B colors none of them lies above the metals-free line; indeed, the most extreme star appears to be HD140283 with a U-B=-0.28* (and which still possesses a small line correction). There is the additional significant point that the compensated colors of both the sub-dwarfs lie on the metals-free main-sequence. The star HD140283 is down in metals abundance by roughly a factor of 25 from the sun and a factor of two of HD19445. (Greenstein and Aller 1959). It is well known that the stellar radius is insensitive to changes in the interior opacity or the helium abundance but is quite sensitive to the presence of a convective envelope which in turn affects primarily the effective temperature altering the luminosity only slightly. The lower metals abundance of the sub-dwarfs may tend to increase the Balmer discontinuity producing a fainter U-B. The fact that these stars give agreement with the metals-free line implies that either the changes in log g (which produces predominantly a U-B difference by also changing the discontinuity) resulting from a convective envelope variation and the Balmer discontinuity resulting from abundance differences are small or produce cancelling effects. This can also be inferred from Figures 18 and 19 where the observed discontinuities are compatible with the systematics of the models.

The color-magnitude diagram offers a potentially stringent indication of the extent to which the positions of the sub-dwarfs may be explained by line

* Derived from more accurate measures recently by G. Abell.

blanketing. This subject although somewhat beyond the realm of this investigation is a logical extension of the work in this chapter and is discussed briefly. The problem of sub-dwarfs is currently being studied by other investigators, notably Code, and a more sophisticated treatment of the subject which also takes cognizance of the effect of metallic deficiencies on stellar interiors must await a later date. Again, all that can be ascertained here is solely the effect of line blanketing.

If one could plot all the stars on a bolometric magnitude-effective temperature diagram the blanketing effect per se would be non-existent. By using Figure 21 or Table XV and including the small effect of blanketing on the absolute visual magnitude one obtains a tantamount result by translating the sub-dwarfs for the prescribed distances along their respective color-magnitude blanketing line. The residuals between the corrected positions and the main-sequence line may be explained as due to departures of the sub-dwarfs from the normal main-sequence mass-effective temperature law.

The absolute magnitude changes through the competing effects of the lines and the continuous flux temperature. In the visual response system it is found from Tables VI and XIII that increasing the flux temperature produces $M_V = -0^m.08/100^\circ$ k. On the other hand, the flux removed by the lines produces a change in M_V of $0^m.01$ in σ Boo, $0^m.03$ in π^3 Ori and 110 Herc, $0^m.06$ in β Com, $0^m.07$ in the sun, $0^m.08$ in 51 Peg and zero for the other stars. In the sun, for example, the increase in flux temperature due to the presence of lines is about 200° k and therefore, the net change in M_V is roughly $+0^m.1$ if all the lines are removed; in any case, the effect is small because of the condensed scale of the M_V ordinate. The effect is shown by the slight slope of the blanketing lines shown on the color-magnitude diagram in Figure 22.

The color-magnitude blanketing lines shown in Figure 22 have been constructed in the above manner using the normal and metals-free main-sequence UBV relations. The lower curve drawn through the terminal points of these lines represents the main-sequence of metals-free stars if the blanketing effect only is operative on this basis. Main-sequence stars of all abundances should lie above this curve. By use of the extrapolated models this curve has been extended somewhat as shown. The normal main-sequence exhibited here is the age-zero relation (Sandage (1957)); the location of the metals-free main-sequence is therefore dependent on this relation.

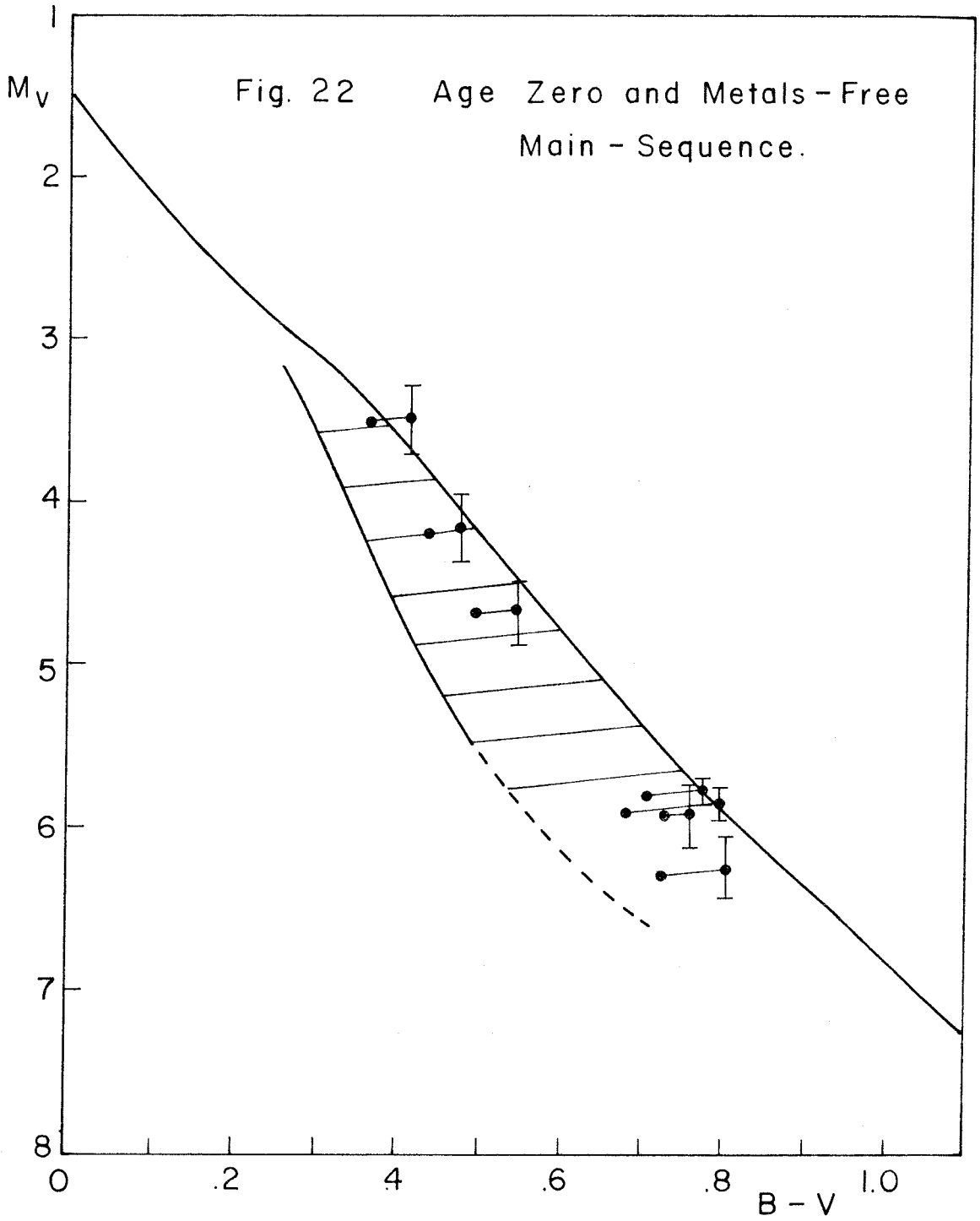
Fig. 22 Age Zero and Metals-Free Main-Sequence.
M_V
1
2
3
4
5
6
7
8
0
.2
.4
.6
.8
1.0
B - V

In practice the use of the color-magnitude diagram to investigate sub-dwarfs suffers from the lack of good parallax determinations for most of the stars of interest. Indeed, for the extreme F-type sub-dwarfs such as HD140283 of which more than ten appear in the high velocity catalog, there is apparently no star whose distance is sufficiently close to give a definitive result. On the other hand, a statistical approach would be of questionable utility because of the small sample size and because the probable errors in absolute magnitude ($\sim 1^m.0$) are perhaps several times the quantities of interest, namely, the residuals.

There are a few mild sub-dwarf stars such as σ Boo whose distances result in absolute magnitude probable errors of $0^m.1$ or $0^m.2$. A list of some of these stars for which U-B colors are available was obtained from recent work by Oke (1959) and presented in Table XVI. The observed and corrected positions of these stars are plotted in Figure 22. Although these few cases offer only a cursory observational comparison, they do seem to suggest that line blanketing is predominantly responsible for the departures of the mild sub-dwarfs from the main-sequence.

Table XVI

HD	B-V	U-B	MV	p.e.	Δ(B-V)
6582	0.69	+0.09	5.9	0.1	0.11
10700	0.72	0.18	5.8	0.05	0.07
64379	0.44	-0.06	4.2	0.2	0.04
89125	0.50	-0.05	4.7	0.2	0.05
128167	0.37	-0.09	3.5	0.2	0.05
144579	0.73	+0.21	6.3	0.2	0.08
154345	0.73	0.26	5.9	0.2	0.03

An interesting project would be to correct all stars with good trigonometric parallaxes to a common UBV main-sequence and use the resulting B-V translations to plot the corrected positions of these stars on a color-magnitude diagram. The remaining vertical spread in the main-sequence relation after allowing for parallax uncertainties would be a measure of the effect of abundance variations arising from causes other than blanketing.

In summary, the effects of blanketing have been demonstrated to be profound, particularly on color-temperature estimates. Correcting observed energy distributions for blanketing leads to reasonable agreement with theory.

It is clear that this investigation is far from comprehensive. Work remains to be done on giants, super-giants, and other astrophysical problems.

REFERENCES

C. W. Allen, 1955. Astrophysical Quantities, p. 116, London: The Athlone Press.

L. H. Aller, 1953. Astrophysics, Vol. 1 New York: The Ronald Press.

J. D. Baum, 1958. Ap. J. 128, 572.

D. Barbier and D. Chalonge, 1941. Ann. d'Ap., 4, 30.

W. K. Bonsack, et al, 1957. Ap. J. 125, 139.

S. Chandrasekhar, 1936. M. N. 96, 21.

S. Chandrasekhar, 1950, Radiative Transfer, p. 304, London: Oxford Univ. Press.

A. D. Code, 1957. Annual Report of Mt. Wilson and Palomar Observatories. p. 45.

A. D. Code, 1959. Stellar Spectra, ed. Greenstein, Chicago: University of Chicago Press. (in press).

C. De Jager and L. Neven, 1957. Recherches Astronomiques De L'Observatoire D'Utrecht, XIII, part 4.

V. M. Goldschmidt, 1937. Norske Videnskaps-Akademi Oslo, Mat.-Naturv. Klasse, No. 4.

J. L. Greenstein and L. H. Aller, 1959. Ap. J. (in press).

W. A. Hiltner and R. C. Williams, 1946. Photometric Atlas of Stellar Spectra, Ann Arbor: Univ. of Michigan Press.

H. L. Johnson and W. W. Morgan, 1953. Ap. J. 117, 313.

P. C. Keenan and W. W. Morgan, 1951. Astrophysics, ed. Kynek, Chap. 1 New York: McGraw-Hill Book Company, Inc.

D. Labs, 1951. Zs. f. Ap. 29, 199.

C. Mark, 1947, Phy. Rev. 72, 558.

E. A. Milne, 1922. Phil. Trans. Roy. Soc. A., 223, 209.

M. Minnaert, G. F. W. Mulders and S. Houtgast, 1940. Photometric Atlas of the Solar Spectrum. Amsterdam: I. Schnabel.

G. Münch, 1946. Ap. J. 104, 87.

P. Naur, 1954. Ap. J. 119, 365.

K. Osawa, 1956, Ap. J. 123, 513.

J. B. Oke, 1959. Ap. J. (in press).

J. C. Pecker, 1951. Ann. D'Ap. 14, 152.

W. G. Roman, 1955. Ap. J. Supp. Vol. 2, 198.

S. Saito, 1956. Contributions from the Inst. of Ap. and Kwasan Obs., Univ. of Kyoto No. 69.

A. R. Sandage, 1957. Ap. J. 125, 435.

M. Schwarzschild, L. Searle and R. Howard, 1955. Ap. J. 122, 353.

M. Schwarzschild, 1958. Structure and Evolution of Stars, p. 139, Princeton: Princeton Univ. Press.

J. Stebbins and A. Whitford, 1945. Ap. J. 102, 318.

J. Stebbins and G. Kron, 1957. Ap. J. 126, 266.

B. Strömgren, 1944. Publikationer og mindre Meddelelser fra Københavns Observatorium, No. 138.

T. L. Swihart, 1956a. Ap. J. 123, 139.

T. L. Swihart, 1956b. Ap. J. 123, 143.

T. L. Swihart, 1956c. Ap. J. 123, 151.

W. Tifft, 1958. Thesis, California Institute of Technology.

R. Woolley and D. Stibbs, 1953. The Outer Layers of A Star, p. 48 London: Oxford Univ. Press.